Experimental Magnetohydrodynamic Energy Extraction from a Pulsed Detonation

THESIS

Kaz I. Teope, Captain, USAF

AFIT-ENY-MS-15-M-224

DEPARTMENT OF THE AIR FORCE
AIR UNIVERSITY

AIR FORCE INSTITUTE OF TECHNOLOGY

Wright-Patterson Air Force Base, Ohio

AFIT-ENY-MS-15-M-224

EXPERIMENTAL MAGNETOHYDRODYNAMIC ENERGY EXTRACTION FROM A PULSED DETONATION

THESIS

Presented to the Faculty

Department of Aeronautics and Astronautics

Graduate School of Engineering and Management

Air Force Institute of Technology

Air University

Air Education and Training Command

in Partial Fulfillment of the Requirements for the

Degree of Master of Science in Mechanical Engineering

Kaz I. Teope, B.S.A.E., M.B.A.

Captain, USAF

March 16, 2015

AFIT-ENY-MS-15-M-224

EXPERIMENTAL MAGNETOHYDRODYNAMIC ENERGY EXTRACTION FROM A PULSED DETONATION

THESIS

Kaz I. Teope, B.S.A.E., M.B.A.
Captain, USAF

Committee Membership:

Dr. P. I. King
Chair

Dr. F. R. Schauer
Member

Dr. W. F. Bailey
Member

AFIT-ENY-MS-15-M-224

Abstract

The high MWatt power available in a fuel-fed detonation wave, which contains combustion ions in the trailing gas, provides an opportunity for external power extraction via electromagnetically forced charged particle drift. Sets of experiments were accomplished using a pulsed detonation tube, extracting power across a load resistor in an electrical circuit with an applied electric or magnetic field to determine what magnitude of gas conductivity and power extraction could be attained from an unseeded or seeded pulsed detonation driven combustion. Due to the low magnetic field strength, even with flow seeding, the power extracted in this research was not enough for practical use. However, theoretical calculations with higher magnetic field strength and greater gas conductivity than was found in this research show promise for continued research. Future work would entail use of a stronger magnetic field to increase power extraction.

Acknowledgements

Funding for this study was provided by AFRL/RQTC, Wright Patterson AFB, Ohio. Thanks go to the personnel at AFRL/RQTC who did some initial testing on the split magnet device.

Special thanks to the members of AFRL/RQTC who helped me conduct experiments and acquire data, particularly: Mr. Curtis Rice, Dr. Christopher Stevens, Dr. Brian Sell, and Dr. John Hoke.

Thanks goes to Dr. Alan Garscadden who provided invaluable insight into the physical aspects occurring between particles within the detonation tube.

I would also like to thank Dr. Daniel Paxson of NASA Glenn for the design of the magnet device and personnel at NASA for the fabrication and initial testing of the split magnet device.

Kaz I. Teope

Table of Contents

Page

List of Figures

List of Tables

List of Symbols

Symbol	
A	Collection plate area (m^2), Amperes
B	Magnetic field (T)
$\bar{B}$	Average magnetic field strength in split magnet device
$\mathbf{B}$	Magnetic field vector (T)
C	Capacitance (F)
d	Distance between collector plates (m)
E	Electric field (V/m), Load resistor energy (J)
$\mathbf{E}$	Electric field vector (V/m)
$\mathbf{E}_{net}$	Net electric field vector (V/m)
$\mathbf{F}$	Lorentz force vector (N)
f	Detonation pulse frequency (Hz)
I	Current (A)
J	Current density (A/m^2)
K	Loading parameter
M	Mach number
n	Time step (s)
N	Number of discreet time steps per pulse
P	Instantaneous Power (W)
$\bar{P}$	Average load resistor power (W)
$\mathcal{P}$	Power density (W/m^3)
q	Elementary charge of a particle (C)
R	Resistance (Ω)
R_i	Internal resistance of the fluid (Ω)
R_L	Load resistance (Ω)

Symbol	
S	Ohm^{-1} (Siemens)
t	Time (s)
u	Flow velocity (m/s)
uB	Induced electric field (V/m)
$\mathbf{u}$	Flow velocity vector (m/s)
V	Capacitor voltage (V)
V_L	Voltage across load (V)
V_{max}	Maximum plate voltage (V)
V_{OC}	Open circuit voltage (V)
V_p	Voltage across plates (V)
V_s	Source voltage
Δt	Sampling time step (s)
σ	Conductivity (S/m)
τ	RC time constant (s)
ϕ	Fuel-oxidizer equivalence ratio
Ω	Ohms

List of Abbreviations

EXPERIMENTAL MAGNETOHYDRODYNAMIC ENERGY EXTRACTION FROM A PULSED DETONATION

I. Introduction

Pulsed detonation engines (PDE) can provide high power density detonation waves and offer a promising propulsion source for the future. That high power density also provides an opportunity for external energy extraction via magnetohydrodynamic (MHD) action on the free floating particles in post combustion products.

Using a single pulsed detonation tube (PDT), operating with a fuel-oxidizer mixture of hydrogen and air at a 10 Hz detonation pulse frequency will provide 110 kJ of energy per second based on a stoichiometric mixture at 1 atm, 22°C, filling a tube of length 1.85 meters and diameter of 5.08 cm, assuming a heating value for hydrogen of 120 MJ/kg.

Tapping even one percent of 110 kJ could provide practical levels of energy considering that 1.1 kJ of energy per second can power approximately 18, 60 Watt lightbulbs. Noting that only a small amount of energy is required to ignite a hydrogen and air mixture, on the order of 1 μJ[5], implementation of a feasible MHD generator onto a PDE could allow for the ability to self sustain the detonation process at low MHD power extraction values. At high MHD power extraction values, it becomes feasible to provide auxiliary power to other systems connected to the PDE, with possible applications in next generation aircraft.

1.1 Research Objectives

Since the high temperature of PDE combustion can ionize the exhaust flow, experiments using parallel ion collector plates situated inside the PDE were conducted to determine:

- the conductivity of the fluid,
- instantaneous power through a known value load resistor
- energy extracted from the flow across a known value load resistor

under the influence of

- an electric field,
- a magnetic field, and
- a magnetic field with flow seeding.

Power for an MHD generator under certain flow conditions has been determined both theoretically and by simulation[6], and shown, as I will under differing flow conditions, that MHD power extraction across a load impedance varies with the internal impedance of the fluid and depends, in particular, on the magnitude of the applied electric and magnetic fields.

1.2 Assumptions

For my analysis, I assumed the following:

- Changes in atmospheric test conditions are negligible day to day
- Combustion reactants behave as an ideal gas
- Combustion products and reactants behave as a calorically perfect gas

- Conduction for the collection plates occurs only in the direction normal to the plate, all other directions being negligible
- Detonation flow parameters are similar for each detonation
- The temperature of the detonation products does not change significantly with time during a pulse
- The applied electric and magnetic fields are uniform

1.3 Limitations

For my analysis, I was limited by the following:

- Measurements were limited by the output of the data acquisition system (DAQ)
- The electric field strength was limited by the maximum output of the power supply
- The magnetic field strength was limited by the device tested
- Seeding material was restricted to water, sodium chloride (NaCl), and potassium carbonate (K_2CO_3)
- Seeding was done manually and not by direct injection

1.4 Thesis Overview

The purpose of this thesis was to understand, through experimental testing, the non-equilibrium particle flow characteristics during a detonation in a PDT and how those flow characteristics affect the feasibility and use of MHD devices to extract energy from high power density detonations.

Chapter 2 discusses previous work done as it pertains to MHD research, specifically, MHD flow augmentation and MHD power extraction. Chapter 3 covers the experimental setup and mathematical models used for determining the conductivity of the fluid, instantaneous power through a known value load resistor, and energy extracted from the flow across a known value load resistor. Chapter 4 covers the analysis and results of experimental testing using the setup and methods covered in Chapter 3. Chapter 5 summarizes the thesis, including some recommendations for future research.

II. Prior Work in MHD and Pulsed Detonation

Research in MHD and pulsed detonation has fallen into two broad areas of study. The first area is MHD flow augmentation where the intent is to change the bulk flow velocity. The second area, the area in which this thesis research pertains, is MHD power extraction where the intent is to extract power out of a gaseous, ionized flow. This chapter contains a brief overview of both areas along with some brief discussions on electromagnetics and flow seeding work.

2.1 Basic Electromagnetics

Resistor-Capacitor Circuits.

A resistor-capacitor (RC) circuit is a circuit containing any number of resistors and capacitors and a voltage source. Figure 1 shows an example of a RC circuit with one resistor and one capacitor.

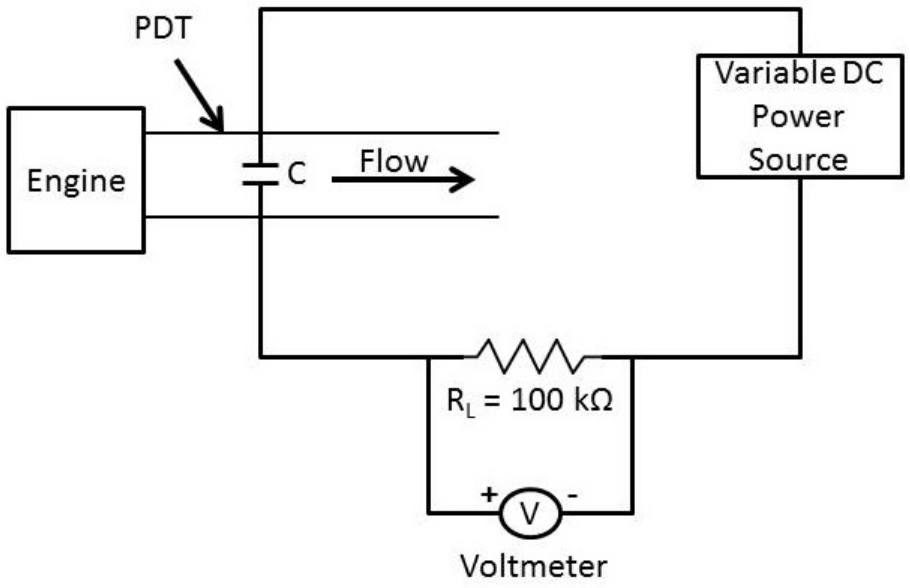

Figure 1. RC electrical circuit

A capacitor in series with a resistor as shown in Fig. 1 is subject to exponential change of electrical charge on the plates. This exponential change exists due to Kirchoff's Voltage Law which states that the sum of the voltages around any closed circuit is zero and the definition of current as the change of charge with time. The equation for a charging capacitor is given by

$$\mathrm{V} = \mathrm{V}_{max}(1 - e^{\frac{-t}{\tau}}) \tag{1}$$

where V_{max} is the maximum voltage on the capacitor and τ is the time constant defined as R×C. The equation for a discharging capacitor is given by

$$\mathrm{V} = \mathrm{V}_{max}e^{\frac{-t}{\tau}}. \tag{2}$$

Equations 1 and 2 result in voltage plots of capacitor plate voltage which look something similar to Fig. 2. It will be seen that the collector plate voltage plots from experimental data taken in this thesis will follow voltage profiles similar to Fig. 2.

Notice the initial section in Fig. 2 shows exponential decay consistent with Eq. 2 with a time constant of approximately 70 μs with resistance and capacitance values that equal that time constant and the terminal section in Fig. 2 shows exponential growth consistent with Eq. 1 with a time constant of approximately 650 μs with resistance and capacitance values that equal that time constant. The exponential curves in Fig. 2 show how changing the time constant can change the charge and/or discharge rate of the capacitor.

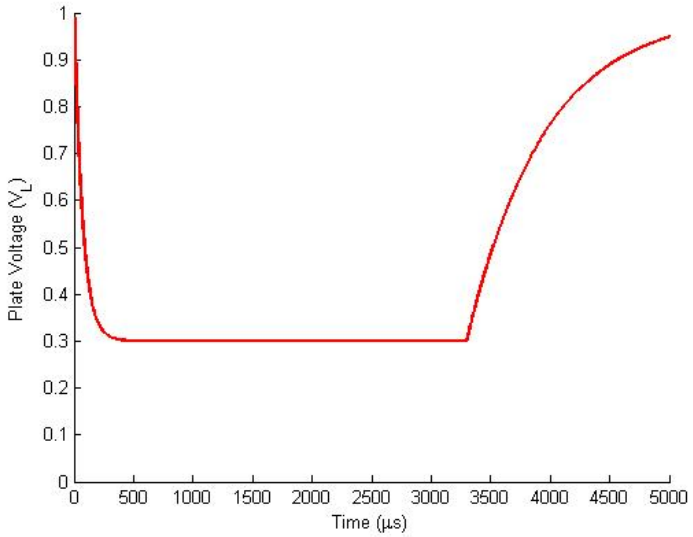

Figure 2. Capacitor plate voltage for a charging and discharging capacitor in an RC circuit

Conductivity.

The conductivity of the fluid in a PDT is of particular importance when discussing MHD power extraction because it is directly related to the amount of energy that can be extracted using an MHD device. The output power density of a MHD generator is directly proportional to the electrical conductivity and flow velocity squared[7]. Since conductivity is a function of the capacitor plate voltage, it is possible to determine an equation for capacitance knowing conductivity. However, the value of conductivity is more relevant than capacitance since capacitance is a material property of the fluid between the collector plates while conductivity is a thermodynamic flow property of the conductive fluid in the PDT. Conductivity has been of interest to other researchers and been calculated from their measurements[1, 2, 6–10]. Simulated values seen in some of the research shows that cesium seeding (0.0002 mole fraction) can achieve conductivities of 15 mho/m[1, 6].

Conductivity of a gas is largely dependent on three factors: the constituents of the gas, the pressure of the gas, and the temperature of the gas. Different gases have

different conductivities. Differences for equilibrium diatomic nitrogen and equilibrium diatomic oxygen are shown in Tables 1 and 2, respectively[3].

Table 1. Electrical conductivity of equilibrium nitrogen (in mhos/cm)[3]

Temperature	Pressure (atm)	
(°K)	1	10
3000	4.25×10^{-10}	$7.56. \times 10^{-11}$
4000	6.34×10^{-6}	1.13×10^{-6}
10000	27.3	21.9

Table 2. Electrical conductivity of equilibrium oxygen (in mhos/cm)[3]

Temperature	Pressure (atm)	
(°K)	1	10
3000	1.9×10^{-7}	4.81×10^{-8}
4000	1.0×10^{-3}	1.55×10^{-4}
10000	28.7	25.7

Tables 1 and 2 show the effect of temperature and pressure on the conductivity of equilibrium nitrogen and oxygen, respectively. As temperature increases, conductivity rises likely due to the increased dissociation of the nitrogen molecules. As pressure increases, conductivity decreases likely due to the increased number density of particles.

2.2 PDEs

PDE Background.

PDEs are engines that use detonation pulses to create thrust. As such, PDEs offer significant advantages over other propulsion alternatives, such as increased thermodynamic efficiency and no moving parts in the tube[1]. For reference, Fig. 3 shows a schematic

of a PDT[1]. The tube in Fig. 3 has a 2.54 cm diameter with two pressure transducers for measuring detonation wave strength and wave speed. Fuel-oxidizer mixture is oxy-acetylene, injected at one end of the tube. Near the open end of the tube, seeding material (cesium-hydroxide/methanol spray) is added to the tube. Additional test sections and MHD channels were added to the open end of the tube for testing[1].

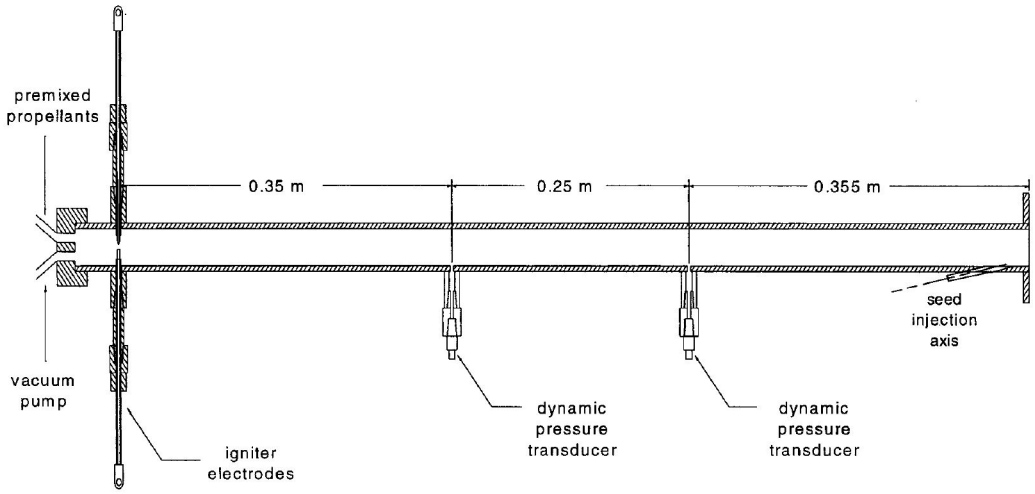

Figure 3. Example schematic of PDT[1]

Detonation Pulse.

While the detonation wave travels down a PDT rapidly ($\sim$ 1 ms for a 2 meter long tube), the detonation process can be visualized as occurring in steps outlined in Fig. 4. The detonation process begins with pre-filling of the tube with fuel and oxidizer to a specified fuel-oxidizer equivalence ratio, ϕ. No detonation is occurring at this time (Fig.4a). The next step is the initiation of the detonation process. Various efforts have been made to study the effects of detonation initiation in a PDT; however, such studies are not the focus of this thesis[11]. Detonation initiation begins with a spark at one end of the tube (Fig. 4b). After the spark, a detonation may not necessarily be present. However, the fuel-oxidizer mixture will begin by deflagrating and creating initial ionization. With detonable mixtures, the detonation forms later down the

PDT (<46 cm for hydrogen and <92 cm for ethylene), and a detonation wave forms and begins to travel down the PDT with a highly ionized region directly behind it as indicated in Fig. 4b. With the collector plates located 1 meter from detonation initiation, after approximately 0.5 ms time, the detonation wave makes contact with the collector plates and a signal is read by the DAQ (Fig. 4c). Initial contact with the collector plates is defined as time zero.

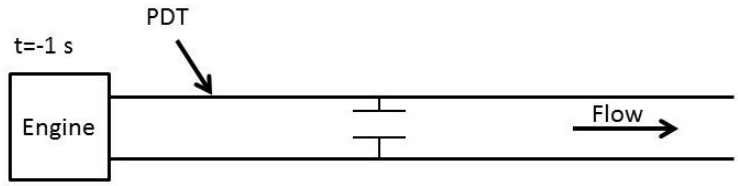

(a) Pre-filling

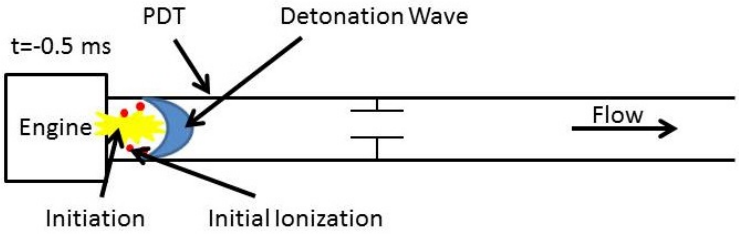

(b) Detonation initiation

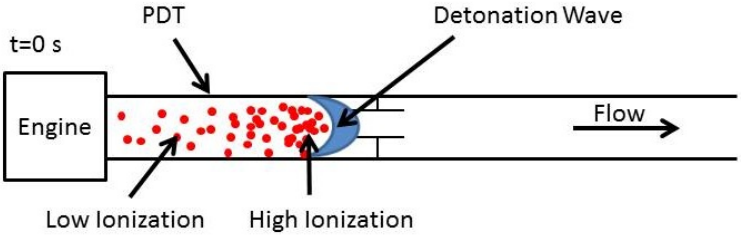

(c) Detonation wave contact with plates

Figure 4. Detonation pulse with time

Numerical simulations of the flow field as it changes with time have also been accomplished to describe the flow characteristics within a detonation tube[12].

PDE Research.

Modern PDE development has been in ongoing since 1986. Development roadmaps and current development, as of the time of the writing of this thesis, have been discussed in previous works[13, 14]. Significant amounts of research have been done with respect to PDEs to include such things as detonation initiation[15] and performance optimization[16, 17] among other things.

As noted in other works, the high power density in a PDT makes it an attractive candidate as a propulsion device and for energy extraction[10]. PDE testbeds have been developed for use in multiple laboratories to include NASA Marshall Flight Center[18].

2.3 MHD

MHD Background.

MHD was recognized by Michael Faraday as early as 1831. The concept of MHD is based on the equation describing a Lorentz force,

$$\mathbf{F} = q(\mathbf{u} \times \mathbf{B} - \mathbf{E}) \tag{3}$$

The Lorentz force describes how a charged particle will move in the presence of an electric and/or magnetic field. MHD devices capitalize on this force by inducing movement in a conductive fluid by means of an externally applied electric field or an induced electric field by means of an externally applied magnetic field, given by $\mathbf{u}\times\mathbf{B}$ in Eq. 3. The net electric field imposed on a charged particle due to an induced electric field by means of an externally applied magnetic field is

$$\mathbf{E}_{net} = \mathbf{u} \times \mathbf{B} - \mathbf{E} \tag{4}$$

Equation 4 describes how a magnetic field vector coupled with a velocity vector induces an electric field indicated by the term $\mathbf{E}_{net}$.

Knowing that the induced electric field is a function of the magnitude of the magnetic field, a device that could use a stationary magnetic field to induce an electric field and induce currents through a load resistor, could then use that current to power another device or store energy for later use. Figure reffig:mhdgen shows an example MHD generator from 1973[2].

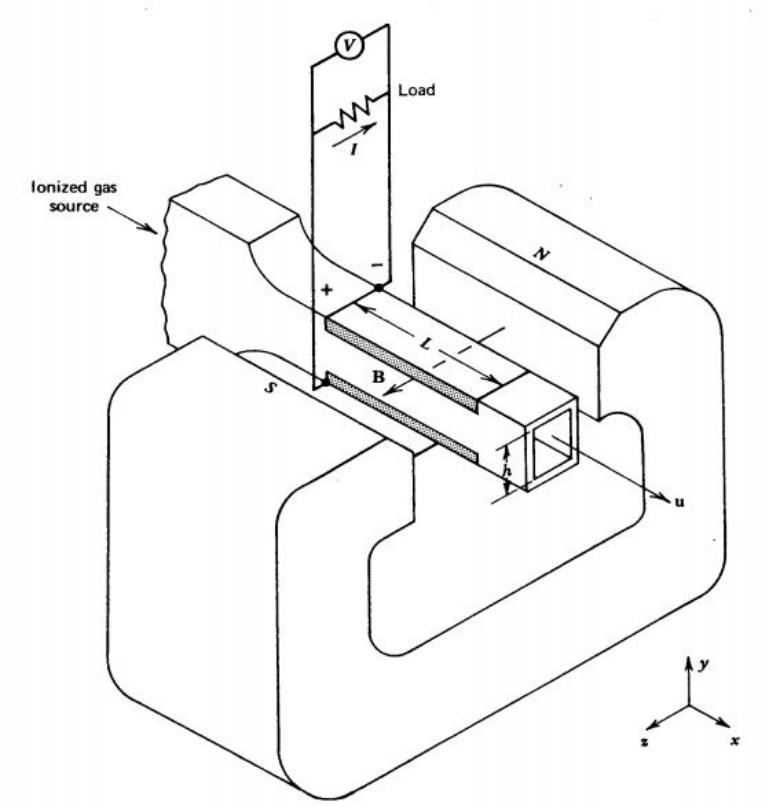

Figure 5. Simple MHD generator[2]

Figure 5 shows a simple MHD generator in the form of a continuous electrode Faraday generator. In Fig. 5, the magnetic field, B, along the z-axis, is applied across the conductive gas with velocity, u, oriented along the x-axis. An electric field is induced in the direction perpendicular to both u and B corresponding with the positive y-axis. The electric field drives an electric current between two conducting

electrodes located above and below the channel[2]. In order to maximize the electromotive effect of the magnetic field on charged particles in the conductive fluid, the magnetic field is oriented orthogonal to the bulk velocity of the conductive fluid. Furthermore, in order to maximize the collection of charged particles by the MHD device, the collection plates are oriented orthogonal to both the bulk velocity and the magnetic field to create the largest induced electric field.

Despite different applications, and regardless of whether a MHD device is used for flow augmentation or power extraction, the physical form of many MHD devices are similar (Fig. 5).

MHD Flow Augmentation Research.

MHD flow augmentation consists of applying both a magnetic field and an electric field across a conductive fluid to generate an electromotive force in line with the bulk flow velocity since neither field alone applied across a conductive fluid can generate an electromotive force in line with the bulk flow velocity (see Eq. 3). An increase in the bulk flow velocity at the exit of a propulsion device could increase the thrust produced. Simulations have shown that impulse gains of up to 6% per cycle were possible[19].

MHD with Different Gas Mixtures.

Both experimental and simulation efforts have shown how different gas mixtures can change the power generation of an MHD device[20, 21]. One such effort studied the electromagnetic effect of seeded argon through a Faraday MHD accelerator[20]. This effort showed via simulation that an argon seeded flow could be accelerated by the Lorentz force (Eq. 3) due to an externally applied voltage[20].

Other researchers performed a numerical simulation of flow augmentation on

an air-plasma gas using a continuous Faraday MHD accelerator[21] building upon the previous work with argon seeding[20]. The air-plasma work showed that under constant loading factor and constant current density, an MHD accelerator with Faraday electrode configuration (Fig. 5) was able to increase the flow velocity of the air-plasma mixture and that higher velocity gains were seen in their constant loading factor case[21].

MHD Power Extraction Research.

MHD power extraction consists of applying a magnetic field and/or an electric field (to simulate a magnetic field) across a conductive fluid in order to extract energy from the flow[1, 6, 9, 10]. The energy extracted can be used to self sustain the PDE, be stored, or at high extraction values, provide power for systems attached to the PDE[1, 6, 9, 10].

Numerical Simulations.

Numerical simulations of energy extraction characteristics for a pulse detonation engine coupled with a MHD generator have been conducted[9, 22]. Energy extracted across a load scaled favorably with length of the PDE (which correlates directly with the mass of propellant and propulsive energy from the detonation) and with increasing magnetic field[9]. However, energy extracted did not scale with the square of magnetic field magnitude as theory would suggest[9]. The magnetic field was simulated to be 2 T[9], higher than that of the work presented here ($\bar{B}$ $\sim$0.281 T).

Flow Seeding.

Various experiments have been conducted to determine the effect of flow seeding on MHD power extraction. Numerical simulations of the flow behavior and performance

for a pulse detonation driven MHD generator with flow seeding have been accomplished[7]. These experiments used a hydrogen-air fuel-oxidizer mixture seeded with cesium and found numerically that addition of nozzles to the generator can provide significant improvements in performance of the MHD generator[7].

Experiments conducted using an oxy-acetylene fuel-oxidizer mixture seeded with a cesium-hydroxide/methanol spray showed peak power extraction across a load impedance between 5-10 Ω[8]. However, no comparison was made to a an unseeded case. These experiments were accomplished by applying a voltage across two collector plates and the effective magnetic field strength calculated. The effective magnetic field strength varied between 0.6—4.2 T[8]. Energy density was found to range from 10-10^3 J/m^3 for the effective magnetic field strength noted above[8]. This research[8] used a continuous length Faraday channel similar to what was done with other researchers[10] and this thesis.

As noted before, flow seeding in an argon gas showed favorable results for electromotive effects[20]. Simulations adding 0.5% mole fraction cesium atoms and ions to the initial mixture have been done to determine the seeding effect[19]. Those same simulations showed conductivity on the order of 1 kmho/m could be achieved with appropriate optimal seed choice, mole fraction, and seed introduction[19]. Cesium, however, was not used as a seeding material in this thesis due to concerns about its reactivity with other gas constituents. The experiments in this thesis used NaCl and K_2CO_3.

III. Methodology

Chapter 3 covers the experimental setup for the three phases of research as well as the mathematical models used in calculating the results discussed in Chapter 4.

3.1 Experimental Methods

The experiments were accomplished in three phases

- Phase 1: The PDT was run with a parallel plate collector system with only an applied source voltage to induce electron movement from an electric field.
- Phase 2: The PDT was run with a split magnet device of centerline stationary field strength of approximately 0.281 T to induce electron movement.
- Phase 3: The PDT was run with a split magnet device of centerline stationary field strength of approximately 0.281 T with flow seeding of K_2CO_3 to increase the conductivity of the flow.

Each of the three phases were tested with three different fuel-oxidizer mixtures: hydrogen-air (H_2-Air), ethylene-air (C_2H_4-Air), and ethylene-nitrous oxide (C_2H_4-N_2O) in a single PDT, with one exception. In the interest of testing time, H_2-Air was not tested for phase three since energy extraction from C_2H_4-Air was found to exceed that of H_2-Air. See Table 3 for a summary of the phases of testing.

Equilibrium Characteristics.

Table 4 summarizes the different detonation characteristics for each of the three fuel-oxidizer mixtures. The detonation energy ($\phi = 1$), found in Table 4, is only based on two parameters: the volume of the tube and fuel-oxidizer mixture. The calculation

Table 3. Test Phase Summary

	Phase 1	Phase 2	Phase 3
Fuel-Oxidizer	E-field	B-field	B-field + seed
H_2-Air ($\phi = 1.0$)	X	X	
C_2H_4-Air ($\phi = 1.2$)	X	X	X
C_2H_4-N_2O ($\phi < 1.0$)	X	X	X

for detonation energy uses the ideal gas law and assumes a pressure of 1 atm and temperature of 22°C.

Table 4. Tube Parameters for Different Fuel-Oxidizer Mixtures

		Tube Volume (m^3)		Energy Per Pulse (kJ)	
Fuel-Oxidizer	LHV (MJ/kg)	Phase 1	Phase 2 & 3	Phase 1	Phase 2 & 3
H_2-Air	120.0	3.76×10^{-3}	2.59×10^{-3}	11.0	7.6
C_2H_4-Air	47.2	4.27×10^{-3}	2.91×10^{-3}	15.3	10.4
C_2H_4-N_2O	47.2	2.92×10^{-3}	6.16×10^{-4}	22.8	4.8

The detonation temperatures found in Table 5 were all found using Chemical Equilibrium with Applications (CEA), a chemical equilibrium code[4]. For reference, the detonation temperature of C_2H_4-Air ($\phi = 1.2$) is 2980 K[4]. Speed of sound was calculated by CEA[4] and is also found in Table 5. Equilibrium electron density found in Table 5 for the three fuel-oxidizer mixtures at $\phi = 1$ were calculated from the mass fractions given by CEA[4]. It is important to note that for all values found in Table 5 are for equilibrium conditions and not representative of the transient, non-steady flow seen in pulsed detonation.

Table 6 shows the particle density of major constituents for equilibrium detonation for the three different fuel-oxidizer mixtures as calculated by CEA[4].

Again, it is important to note that for all values found in Table 6 are for equilibrium

Table 5. Equilibrium Detonation Characteristics for Different Fuel-Oxidizer Mixtures[4]

Fuel-Oxidizer	Temperature (K)	Speed of Sound (m/s)	Electron Density ($1/m^3$)
H_2-Air	2942	1091.1	8.01×10^{16}
C_2H_4-Air	2923	1005.2	7.99×10^{16}
C_2H_4-N_2O	3791	1196.4	1.40×10^{19}

conditions and not representative of the transient, non-steady flow seen in pulsed detonation.

Parallel Plate Collector System.

A diagram of the circuit for the phase 1 parallel plate collector system is shown in Fig. 1. Source voltage, supplied by an external power source, was varied from 0.5 V to 11.5 V in 0.5 V increments and applied to the upper electrode with the lower electrode grounded. Voltage measurements were taken across a 100 kΩ resistor.

The collector plate electrodes indicated by C in Fig. 1 were located inside a 5.08 cm diameter polyvinyl chloride (PVC) tube attached on both ends by metal tubing. Figure 6 shows a picture of the phase one test section with electrodes inside the tube indicated by white arrows. The PVC test section is 30 cm in length with the center of the capacitive plates located at 15 cm. The collector plates are mounted to the PVC tube via a set of holes drilled in the PVC and a set of screws attached to the collector plates. The collector plates are 5.08 cm long and 1.27 cm wide resulting in a collection area for the two plates of 6.45 cm^2.

Split Magnet Device.

Electron movement was induced by a stationary magnetic field provided by a split magnet device attached to a PDT. (There was no applied electric field.) Figure

Table 6. Particle Density ($1/m^3$) of Major Constituents for Equilibrium Detonation for Different Fuel-Oxidizer Mixtures[4]

	Fuel-Oxidizer		
Particle	H_2-Air	C_2H_4-Air	C_2H_4-N_2O
H_2O	1.15×10^{25}	5.52×10^{24}	7.56×10^{24}
N_2	2.46×10^{25}	3.31×10^{25}	3.80×10^{25}
O_2	2.94×10^{23}	6.86×10^{23}	2.89×10^{24}
OH	7.40×10^{23}	5.93×10^{23}	4.29×10^{24}
NO	2.93×10^{23}	5.08×10^{23}	2.62×10^{24}
H_2	1.23×10^{24}	3.43×10^{23}	2.28×10^{24}
H	2.30×10^{23}	1.15×10^{23}	2.28×10^{24}
O	7.86×10^{22}	1.13×10^{23}	2.28×10^{24}
CO	0	1.89×10^{24}	9.46×10^{24}
CO_2	0	1.15×10^{25}	3.64×10^{24}

7 shows a diagram of the split magnet device circuit. Power output of the split magnet device was measured by the change in voltage across varying resistances ranging from 100 Ω to 100 kΩ.

The split magnet device has a 2.29 cm inner diameter. Two conductive plates of length 15.2 cm run inside the device in the axial direction normal to the magnets to maximize the induced electric field from the ionized combustion gases as described by Eq. 4. Figure 8 shows a picture of the phase two and three test section attached to the end of a 2.54 cm diameter stainless steel PDT. The entrance to the test section is indicated by the white arrow. The test section and split magnet device follows to the left of the white arrow.

The split magnet device has two rows of 3-5.08 cm square magnets, above and below the flow, running along the axial flow direction. From a traversing gauss meter,

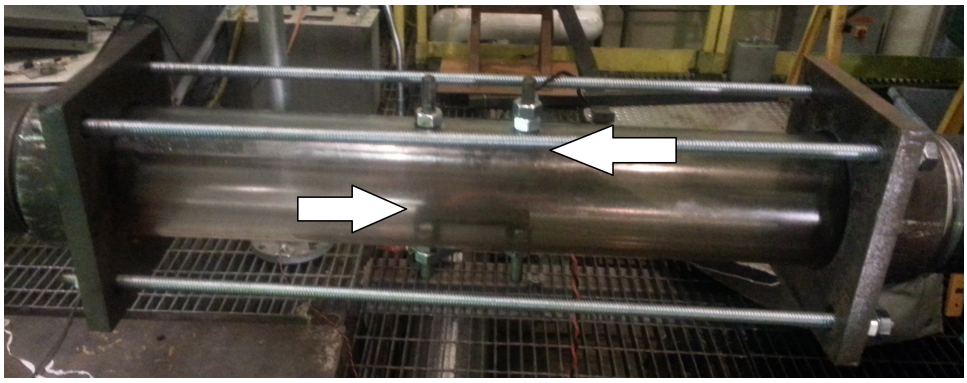

Figure 6. Parallel plate collector test section used in phase 1

the magnetic field strength was measured at 1.27 cm increments beginning at the exit of the split magnet device channel. The magnetic field strength was measured along the centerline of the channel. Three traverses were made and the results averaged. Figure 9 shows the magnetic field measurement for the split magnet device.

Figure 9 shows the peak value of 0.3473 T occurs near the axial center. I used the value 0.2813 T, the average magnetic field strength of the split magnet device, $\bar{B}$, for calculation of conductivity in phase two and three experiments. The average value within the center of the split magnet device is 0.3445 T for reference.

The conductive plates in the split magnet device were arched to follow the curvature of the 2.29 cm inner diameter. The conductive plates spanned 60°on each side of the tube with a corresponding arc length of 1.197 cm. The conductive plates were 15.24 cm long resulting in an area for the conductive plates of 18.24 cm^2. The average distance between the conductive plates was 2.183 cm.

3.2 Experimental Setup for Hydrogen-Air and Ethylene-Air

All experiments done with H_2-Air and C_2H_4-Air used a 5.08 cm diameter PDT. Fuel, oxidizer, and timing were supplied to the 5.08 cm diameter PDT via an automotive four stroke combustion engine. Figure 10 shows a picture of the engine block with a 5.08 cm diameter PDT attached.

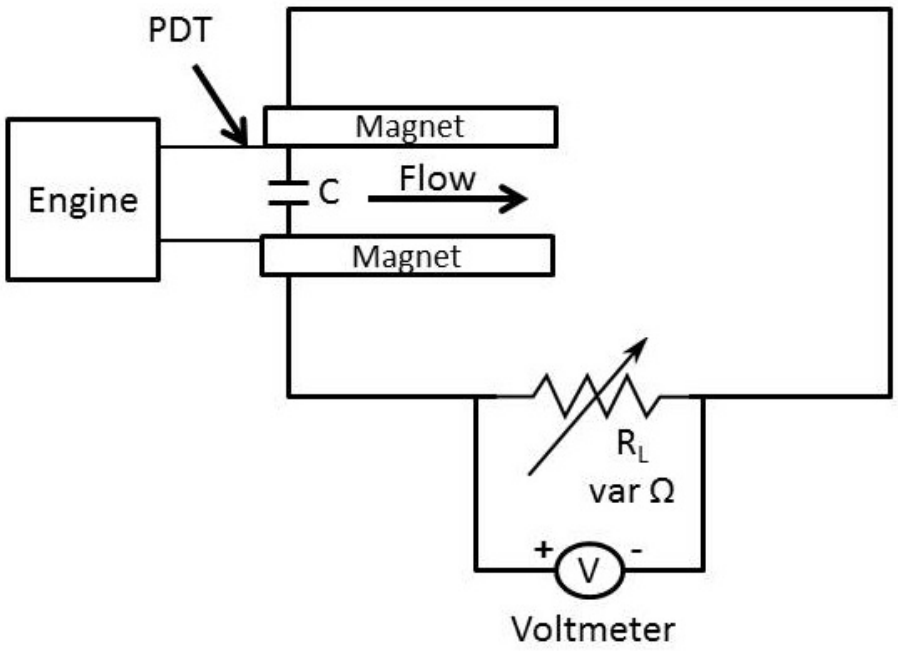

Figure 7. Phase 2 and 3: split magnet system for inducing electron movement in a PDT electrical circuit

Shown in Fig. 10 are the valves that regulate the fuel-oxidizer mixture injection. For both experimental fuel-oxidizer mixtures, detonations were set at a frequency of 10 Hz. A remote DAQ measured the voltage across a load resistor, R_L (see Fig. 1), at a sampling rate of 1 MHz. Shielded wire and a common ground were used throughout the DAQ system to avoid capacitive issues in the measurements.

The PDT without a test section added is 96.5 cm long and 5.08 cm in diameter. The electric and magnetic field test sections were added onto the end of the existing

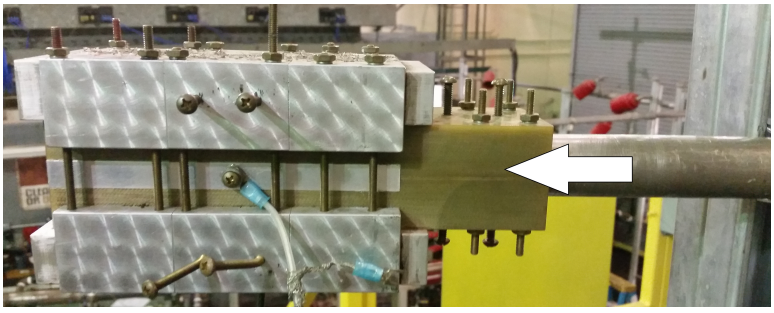

Figure 8. Split magnet device test section used for phases 2 and 3

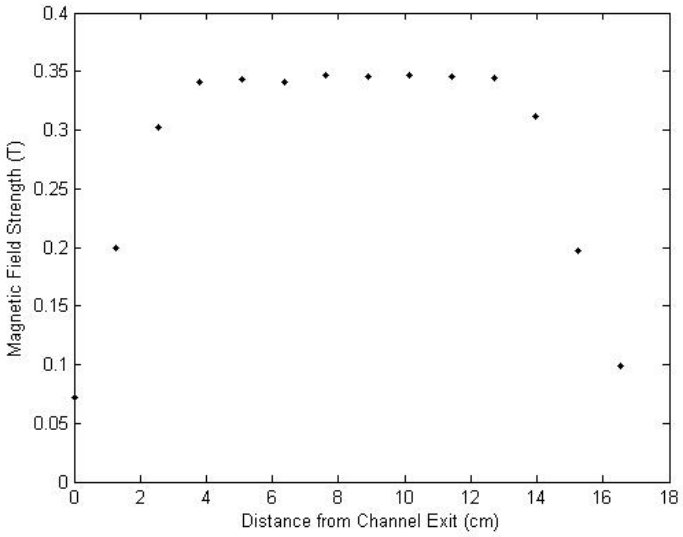

Figure 9. Magnetic field measurement for split magnet device

PDT increasing the length and volume of the tube. The H_2-Air was run at a stoichiometric combustion ratio with a 50% purge fraction. However, the C_2H_4-Air was run at $\phi = 1.2$ because the C_2H_4-Air suffered inconsistent detonation development at lower values of ϕ. Verification of detonation was determined by two ion probes located upstream of the test section at 76.2 cm, and 91.4 cm, respectively. Figure 11 shows the two ion probes located on the 5.08 cm diameter PDT indicated by white arrows. Typical detonation velocities with some small variations were measured at approximately 2000 m/s for all fuel-oxidizer mixtures.

3.3 Experimental Setup for Ethylene-Nitrous Oxide

Testing was restricted to certain diameters of PDTs. The nitrous oxide was only available on a 2.54 cm or 7.62 cm PDT. There was a concern that if the 7.62 cm PDT was stepped down to 2.29 cm to match the diameter of the split magnet device, the detonation pressure would exceed the structural limits of the split magnet device. Thus, all experiments done with C_2H_4-N_2O used a 2.54 cm diameter PDT leading into

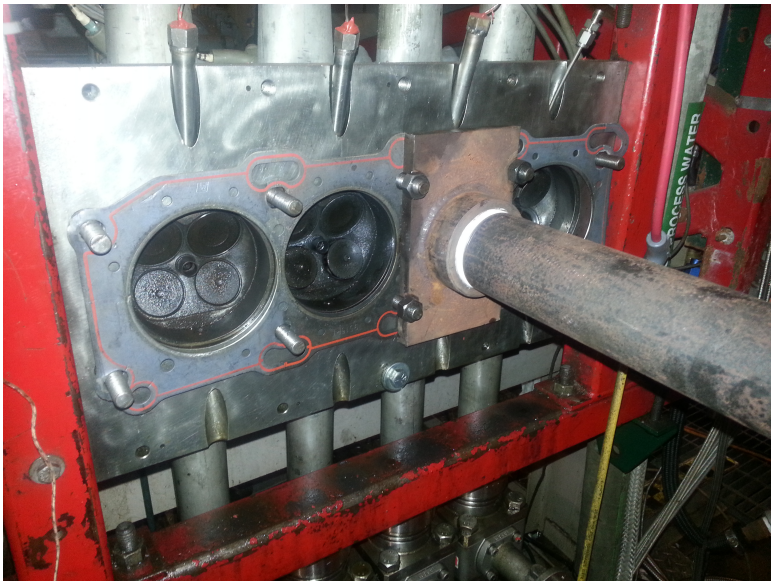

Figure 10. Four stroke engine head with PDT attached

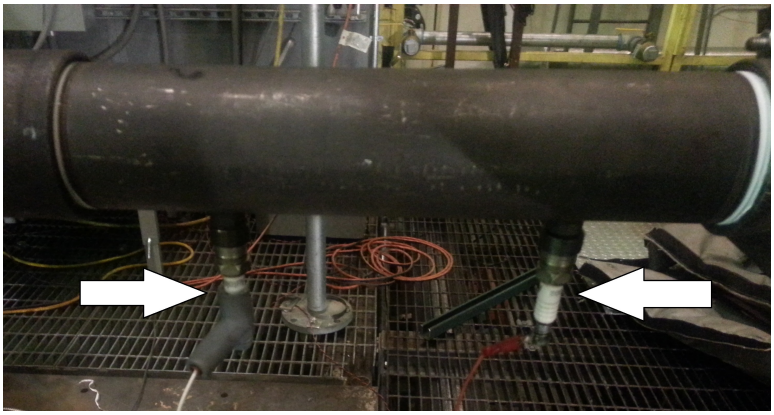

Figure 11. Ion probes for verifying detonation

the test section. Fuel, oxidizer, and timing were supplied to the 2.54 cm diameter PDT via a set of independent valves and fuel/air injectors. Figure 12 shows a schematic of the C_2H_4-N_2O setup.

The C_2H_4-N_2O PDT without a test section was 99 cm in length. From the injectors to 19 cm, the diameter of the tube is 1.27 cm. Between 19 cm and 37 cm, the diameter of the tube increases from 1.27 cm to 2.54 cm in an expansion section. The remainder of the length of the tube (62 cm) is 2.54 cm in diameter. A seeding port was located 86.4 cm from the injectors . Some test cases used this port for manually adding

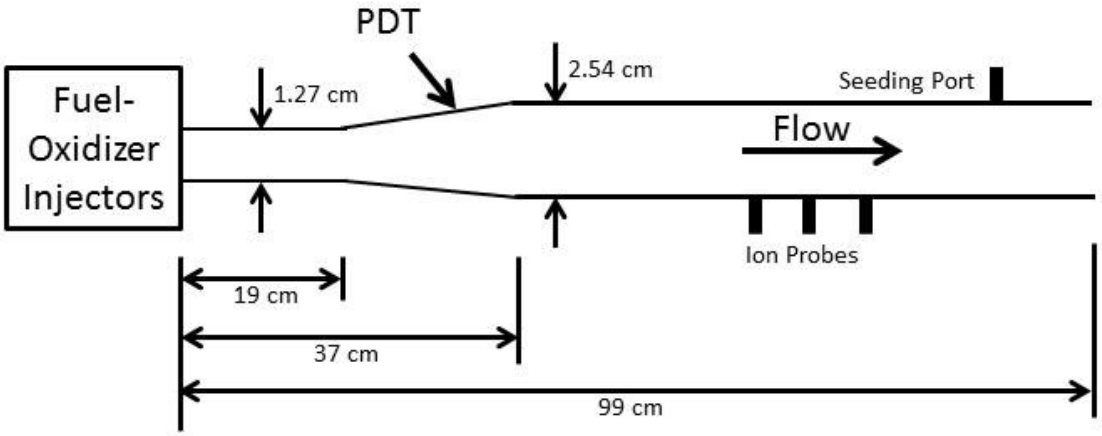

Figure 12. C_2H_4-N_2O schematic

seeding material into the tube prior to detonation.

The parallel plate collector and split magnet device test sections (Figs. 6 and 8) were added to the end of the PDT increasing the length and volume of the tube. The ϕ was varied by controlling the fuel and oxidizer back pressures to the injectors. The fuel-oxidizer mixture is mixed in the PDT and the PDT was overfilled to ensure adequate filling. Verification of detonation was determined by any two of the three ion probes located upstream of the test section at 57.1 cm, 62.2 cm, and 67.3 cm, respectively, shown in Fig. 12. Only two of the ion probes are required to verify detonation; however, three ion probes were available and were used for redundancy. Typical detonation velocities with some small variations were measured at 2000 m/s. A remote DAQ measured the voltage across a load resistor, R_L, attached to the same circuit as phase two (Fig. 7) and to the split magnet device collector plates as in phase two (Fig. 8) at a sampling rate of 1 MHz. Shielded wire and a common ground were used throughout the DAQ system to avoid capacitive issues in the measurements.

Flow Seeding with Sodium Chloride and Potassium Carbonate.

Flow seeding was initially accomplished with two different seeding materials. Flow seeding was done by manually adding either water or saturated aqueous NaCl, with solubility of 360 g/1 kg of water at 25°C[23], into the expansion section of the C_2H_4-N_2O test setup (Fig. 12). The section was removed from the tube and capped on one end while approximately 2 mL of water or a saturated solution of aqueous NaCl was added to the expansion section. The expansion section was coated with the water or NaCl solution and the excess dumped out. A detonation followed shortly after the expansion section was reattached to the tube, minimizing the evaporation of water from the tube. Brief results for the NaCl testing are included in this chapter to help explain the need to change to K_2CO_3 as a seed material. Detailed results for all seeding materials will be presented in Chapter 4.

Initial seeding results using water and aqueous NaCl were found not to yield the expected higher power and energy extracted with seeding, and the seed material was changed to K_2CO_3 which was expected to yield higher power and energy extraction.

The K_2CO_3 was manually added to the PDT into the expansion section (Fig. 12) or through one of the ports (Fig. 12) in the PDT for the C_2H_4-N_2O testing in either 1) saturated aqueous solution, with solubility of 112 g/100 mL of water at 20 °C[24], or 2) as a dry powder salt ($\sim$0.5 g). If added in aqueous form, the PDT was allowed to dry or was dried with a heat gun prior to testing to minimize the degrading effect of water and water vapor seen with the NaCl testing. The amount of seed that was added to the PDT was not accurately weighed; however, approximate amounts added are known.

Fuel to Oxidizer Equivalence Ratio, ϕ.

The effect of ϕ was investigated for the C_2H_4-N_2O. To accomplish these experiments, the PDT was run at the lowest ethylene fuel fraction where detonation could still be sustained as verified by the ion probes in the tube (Fig. 12). Ethylene fuel fractions were then increased until the fuel fraction exceeded the detonable limit and detonation was no longer indicated by the ion probes. For this test, it was beneficial to have three ion probes as it was possible to have no detonation as the exhaust gases passed the first ion probe but to have a detonation form past the first ion probe and be captured by the second and third ion probes. Data was taken for three selected load resistances (100 Ω, 1000 Ω, 10 kΩ).

3.4 Mathematical Models

Electrical Field Model.

By Ohms Law, current is given by

$$I = \frac{V_L}{R_L}. \tag{5}$$

The conductivity of the fluid is given by

$$\sigma = \frac{J}{E} = \frac{I/A}{V_p/d} = \frac{V_L d}{R_L V_p A} \tag{6}$$

where the collector plate voltage $V_p = V_s - V_L$.

Instantaneous power through the load resistor is given by

$$P = IV_L = \frac{V_L^2}{R_L} \tag{7}$$

For very high sampling rates, the energy for an entire pulse is

$$E = \sum_{1}^{N} P\Delta t \tag{8}$$

since $(P_n + P_{n+1})/2 \sim P_n$.

Finally, the average load power is given by

$$\bar{P} = E \times f \tag{9}$$

where f is the PDT pulse frequency, which in these experiments was 10 Hz.

Magnetic Field Model.

In my experiment, E comes from the experimentally measured load voltage, V_L,

$$E = V_L/d \tag{10}$$

With $\mathbf{E}_{net}$ established from Eq. 4, conductivity, power, and energy are computed from Eqs. 6—9. I assumed for calculations that uB and E are uniform, but that assumption is ideal at best, and I estimate an uncertainty in uB, in particular, of about 25%.

The power for the generator shown in Fig. 5 is given by[2]

$$P = \sigma u^2 B^2 K(1 - K) \tag{11}$$

where K is defined as the loading parameter. The value of K that maximizes Eq. 11 is 0.5. The equation for loading parameter is given by[2]

$$K = \frac{E}{uB} \tag{12}$$

Furthermore, K can be defined as

$$K = \frac{E}{uB} = \frac{V_L/d}{V_{OC}/d} = \frac{V_L}{V_{OC}} = \frac{IR_L}{I(R_L + R_i)} = \frac{R_L}{R_L + R_i} \tag{13}$$

where V_{OC} is defined as the open circuit voltage of the circuit in Fig. 1 and in an MHD device is equal to uB×d[2] and R_i is the internal resistance of the fluid. In order to make K equal to 0.5, to maximize Eq. 11, Eq. 13 shows that the load resistance, R_L must match the internal resistance of the fluid, R_i. The effect of matching the impedance of the load to the impedance of the fluid will be seen later in this thesis.

Theoretical maximum MHD power extraction following Eq. 11 from the flow for phase two and three experiments, assuming K = 0.5, is[2]

$$P = \frac{Ad\sigma u^2 B^2}{4} \tag{14}$$

Power density is then[2]

$$\mathcal{P} = \frac{P}{Ad} = \frac{\sigma u^2 B^2}{4} \tag{15}$$

where σ is calculated from Eq. 6 as was done in phase one.

I will use Eqs. 14 and 15 for comparisons with experimental results. Since the split magnet induces electron movement in a direction normal to the flow direction, this movement interacts with the magnetic field and induces a Hall Effect. But as others have done[2, 10], I have considered the Hall effect negligible.

IV. Analysis and Results

The data was post processed in Matlab. Matlab was used to convert the files from the DAQ to usable text files (code provided by AFRL/RQTC). All other code used for analysis was written by the author.

4.1 Phase 1 Results for Applied Electric Field Only

The voltage, V_L, across a resistance of 100 kΩ (R_L) was measured for varying source voltages (see Fig. 1). Twenty-three voltages were tested ranging from 0.5 V to 11.5 V in 0.5 V increments. Three pulses of data (see Fig. 13) were taken for each run for H_2-Air and C_2H_4-Air. One pulse of data was taken for the C_2H_4-N_2O runs since the C_2H_4-N_2O test setup could only create one pulse at a time. Figure 13 shows example profiles for the 1.0 V case for H_2-Air. At a 10 Hz detonation frequency, detonation intervals were 100 ms, of which 5 ms (5000 μs) was comprised of the rise and fall of the voltage signal, as seen in Fig. 13, with time zero corresponding to the instant when the detonation wave makes contact with the collection plates. This type of falling voltage signal was also observed by others[1, 6, 8–10, 18].

For H_2-Air and C_2H_4-Air, in most cases, as seen in Fig. 13, the first pulse was a different signal shape with a lower outlier mean. One possible reason for the displaced first pulse is that the collector plates initially at room temperature were heated by the first pulse such that the second and third pulses created electron movement to the collector plates with presumed higher resistivity. This higher resistivity would account for the higher voltages required to maintain the same current in the circuit. As a result, this work uses only the second pulse to find V_L. It is noted that ensemble averaging did not change the results processed for the second pulse.

The signal shown in Fig. 13 appears to have a three distinct regions. The first

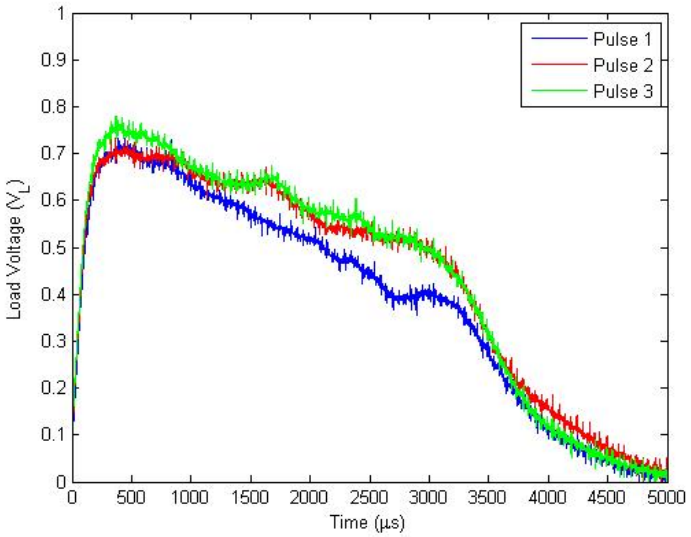

Figure 13. Phase 1: load voltage for a single source voltage, R_L = 100 kΩ, H_2-Air, V_s = 1.0 V

region spans from 0-500 μs where the signal looks like an exponential growth curve. The second region spans from 500-3300 μs and is approximately linear with negative slope. The third and final region spans from 3300-5000 μs and looks similar to an exponential decay curve that quickly falls off to nearly zero. Further clarification comes from an examination of Fig. 14.

Figure 14 shows the plate voltage for the second pulse shown in Fig. 13. In Fig. 14, one can see the effects of the RC circuit in Fig. 1. The three regions in Fig. 13 are the same in Fig. 14 and are sectioned in Fig. 14. Figure 14 approximates the capacitor plate voltage curve in Fig. 2.

The first region in Fig. 14, 0-500μs, can be described as a discharging capacitor with an approximate time constant of 70 μs resulting in an effective capacitance of 0.7 nF. That is when the detonation wave makes contact with the collector plates, which is seen as a step impulse by the plates, the plate voltage drops exponentially as current begins to flow across the plate gap. The highly ionized flow directly behind the detonation wave provides a mode for current to flow maintaining the lower plate

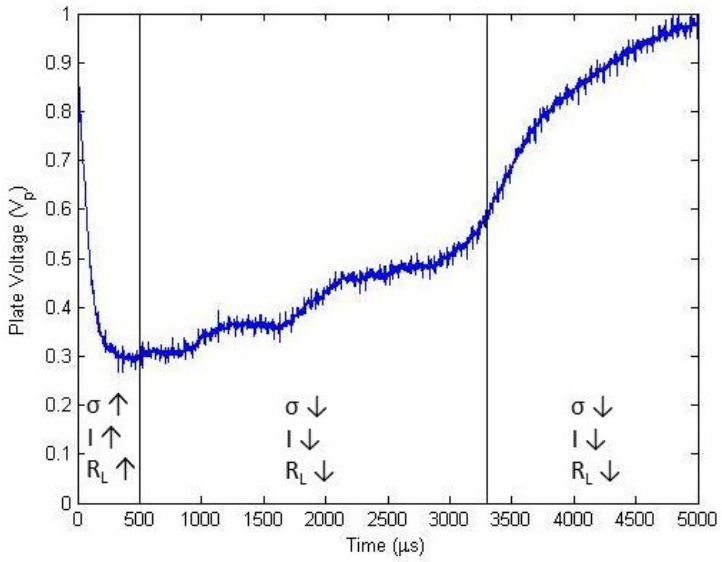

Figure 14. Phase 1: plate voltage for a single source voltage, R_L = 100 kΩ, H_2-Air, V_s = 1.0 V

voltage seen in Fig. 14. However, as time progresses, lesser ionized flow passes the collector plates resulting in lower flow conductivity, less current flow, and higher plate voltage resulting in the effect seen in the second region (500-3300 μs). The third region can be described as a charging capacitor subject to a time constant of approximately 650 μs resulting in an effective capacitance of 6.5 nF. The trends for conductivity, current, and load resistance are annotated in each section of Fig. 14. Assuming that in the third region the fluid is no longer conducting, that indicates a pulse duration of 3300 μs, and further assuming a near sonic ionized gas velocity (∼1 km/s) trailing the detonation wave, this leads to a conductive gas length of 3.3 meters and a corresponding volume for a 5.08 cm PDT of 6.69×10^{-3} m^3. However, the length of the tube prior to the test section is only about 1 meter in length corresponding to a volume of only 2.03×10^{-3} m^3. Further, assuming that the temperature of the combustion products does not vary significantly with time, in order to attain the increased volume, the gas must expand and pressure and density must drop.

For C_2H_4-N_2O, only one pulse of data was taken per run since the test setup

could only signal one pulse at a time. However, repeated pulses of data were taken to ensure repeatability of pulses. Pulses for this fuel-oxidizer mixture did not have differing signal shapes from pulse to pulse as was seen in Fig. 13. It is noted that ensemble averaging did not change the results processed for a single pulse.

Phase 1: Gas Conductivity.

Conductivity is of particular importance because this parameter has direct relation to the current density (Eq. 6) and consequently the energy extracted, which is of interest in this thesis. The conductivity plots in Fig. 15 were found using Eq. 6 and show the conductivity for three of the 23 voltages tested, 3.0 V, 6.0 V, and 11.5 V, for three fuel-oxidizer mixtures. Voltages not shown fell systematically above and between those shown.

In Fig. 15, conductivity falls with time, as seen by other researchers[1]. The author ascribes this to the rapidly falling gas density (and, thus, electron density) of the gas. While the temperature of the combustion products does not vary significantly with time, the pressure falls rapidly with time (see section 4.1 regarding falling pressure and density). Thus, with constant temperature and volume but rapidly falling pressure, the density of the gas will also fall rapidly. In the early region of the data (Fig. 15), the maximum conductivity for the 3.0 V case for all mixtures, is higher than the 11.5 V case suggesting that conductivity decreases with source voltage. Figure 16 shows the normalized load voltage curves for three selected source voltages (3.0 V, 6.0 V, and 11.5 V).

Figure 16 shows that as source voltage increases, the ratio of load voltage to source voltage decreases a similar trend seen in Fig 15a. One explanation for this decrease in load voltage as source voltage increases (Fig. 16) is, as the source voltage increases, the increased electric field increases the charge accumulation on the collector plates.

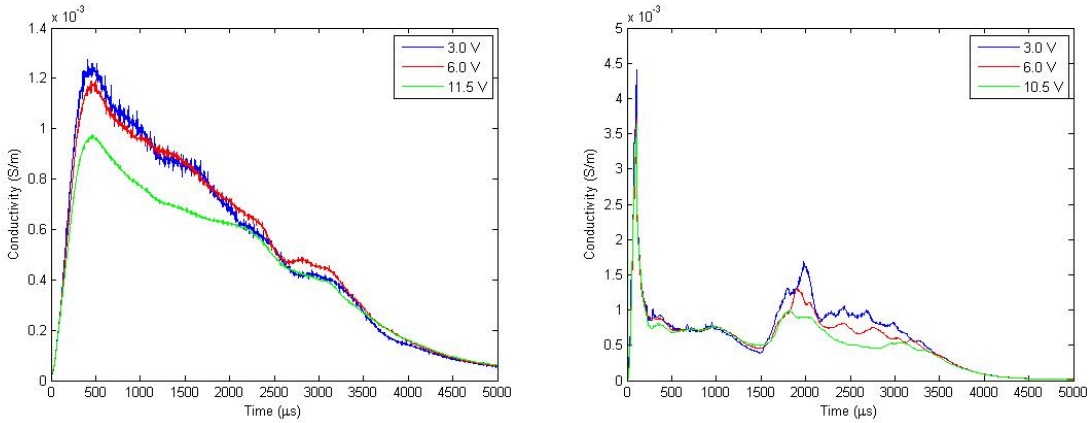

(a) H_2-Air (b) C_2H_4-Air

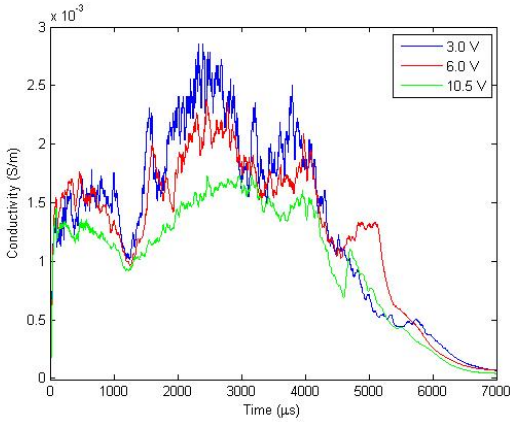

(c) C_2H_4-N_2O

Figure 15. Phase 1: instantaneous conductivity for selected source voltages, R_L = 100 kΩ, mixture specified

This increased accumulation has the effect of increasing the polarization between the plates which creates an area of localized negative charges in front of the positive plate. This localized negative charge field creates a resistance to further negative charge accumulation and further current flow through the fluid. This increased resistance to the current flow has the effect of reducing the current and voltage through the resistor, leading to the drop in conductivity as seen in Fig. 15.

Figure 17 compares the instantaneous conductivity for all three fuel-oxidizer mixtures at the 3.0 V case. Peak values of conductivity for H_2-Air are approximately 0.5 mS/m

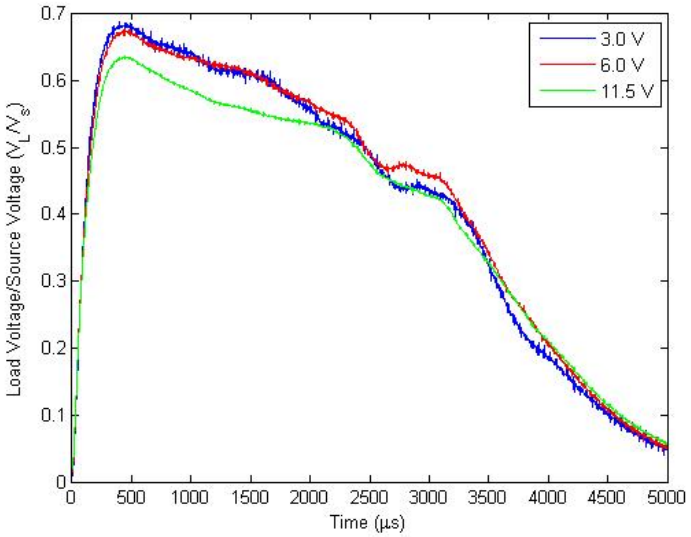

Figure 16. Phase 1: load voltage normalized by source voltage for selected source voltages, R_L = 100 kΩ, H_2-Air

and this value corresponds roughly to the nearly zero value seen in other research[6] for a non-seeded case. Peak values for both ethylene mixtures, were higher than that of H_2-Air with C_2H_4-Air higher (∼4 mS/m) than the C_2H_4-N_2O (∼3 mS/m). C_2H_4-N_2O also has the highest average conductivity over a pulse, followed by C_2H_4-Air and H_2-Air with the least average conductivity.

Instantaneous Power through Load Resistor, R_L.

Figure 18 shows the load power for the 3.0 V, 6.0 V, and 11.5 V source voltages, solved using Eq. 7 for the three different fuel-oxidizer mixtures. In Fig. 18, power, which scales with conductivity (Eqs. 6 and 7), falls with time. Also from Fig. 18, as the source voltage increases the instantaneous power increases since an increase in source voltage increases the instantaneous load voltage, and according to Eq. 7, increases instantaneous power. The maximum instantaneous power value for the 3.0 V, H_2-Air case is 0.525×10^{-4} W and 6.71×10^{-4} W for the 11.5 V case. Similar trends with respect to source voltage were seen in both of the other fuel-oxidizer

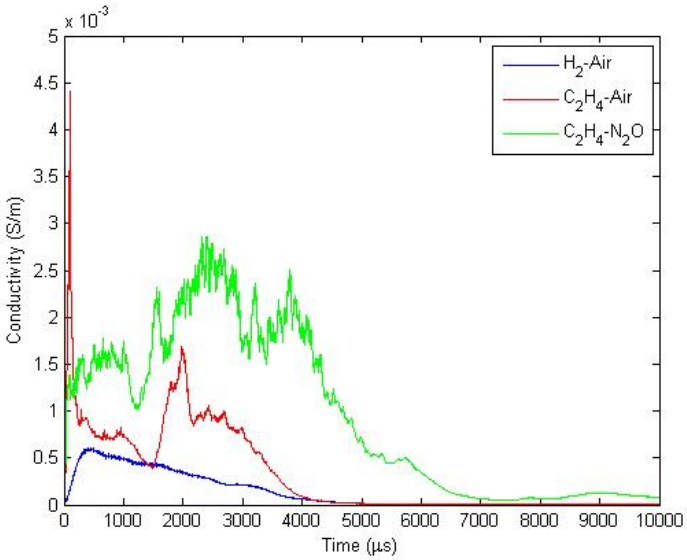

Figure 17. Phase 1: instantaneous conductivity for 3.0 V case, all mixtures, $\mathbf{R}_L$ = 100 kΩ

mixtures tested. Such low values of power extracted seen in Fig. 18 could be increased with higher source voltages up to 100 V have been simulated and tested[1, 6].

Figure 19 shows the instantaneous power for the 3.0 V case for all three fuel-oxidizer mixtures. It is noted that the trends with regard to fuel-oxidizer mixture do not change with source voltage therefore, the 3.0 V case will show the same trends for instantaneous load power with respect to fuel-oxidizer mixture as would the 10.5 V case.

The characteristic drop seen in C_2H_4-Air at approximately 1500 μs was seen for all source voltages as seen in Fig. 18b. C_2H_4-N_2O also showed a drop at approximately the same time ($\sim$1500 μs) also seen in Fig. 18c. H_2-Air did not show this drop seen in the ethylene mixtures (Fig. 18a). Peak values of power from Fig. 19 for H_2-Air of approximately 40 μW are noted. Peak value for the C_2H_4-Air was approximately 80 μW (Fig. 19 but occurred in the first 200 μs corresponding to the conductivity spike seen in Fig. 18b. After the initial spike, the peak value for C_2H_4-Air was approximately 70 μW. C_2H_4-N_2O has a peak value ($\sim$75 μW) similar to

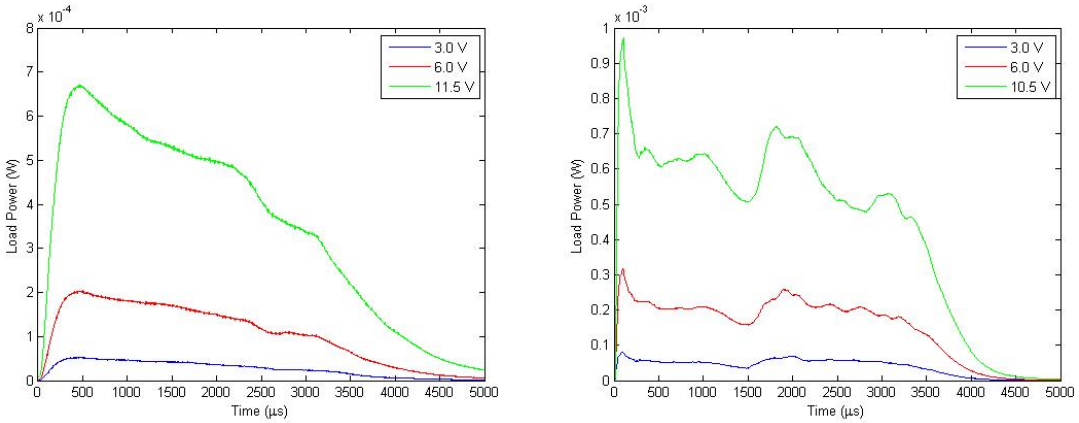

(a) H_2-Air

(b) C_2H_4-Air

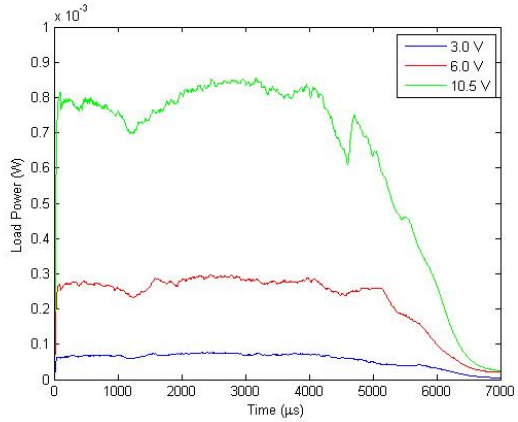

(c) C_2H_4-N_2O

Figure 18. Phase 1: instantaneous load power for selected source voltages, $R_L = 100$ kΩ, mixture specified

that of C_2H_4-Air, suggesting that peak values of power may be unaffected by oxidizer choice. However, the C_2H_4-N_2O has the highest average power over a pulse followed by C_2H_4-Air and H_2-Air with the least average power as seen in Fig. 19.

Energy Extracted through Load Resistor, R_L.

Figure 20 shows the load resistor energy per pulse for the three different fuel-oxidizer mixtures, obtained from Eq. 8. Figure 20 shows that the energy derived from a single detonation increases with source voltage for all three fuel-oxidizer mixtures.

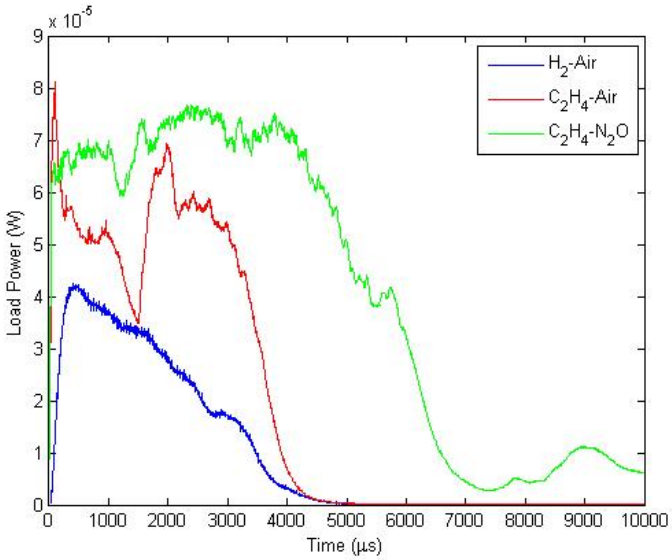

Figure 19. Phase 1: instantaneous power for 3.0 V cases, all mixtures, $\mathbf{R}_L$ = 100 kΩ

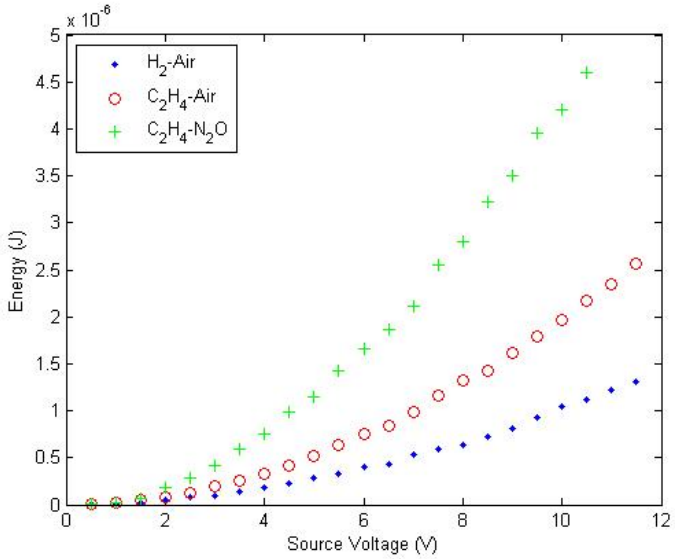

Figure 20. Phase 1: load resistor energy per pulse as a function of source voltage, all mixtures, $\mathbf{R}_L$ = 100 kΩ

At a voltage of 11.5 V for H_2-Air, the energy density (energy per unit volume), is computed to be 1.76 μJ/(1.64×10^{-5}) m^3 (volume of the plate region = 1.64×10^{-5} m^3) = 0.107 J/m^3. Similarly small values were also seen in the other works[1, 6]. The average power, $\bar{P}$, is computed from Eq. 9, and is any of the energy values in Fig. 20 multiplied by 10 (= f). For example, in Fig. 20, the load energy for a 6.0 V source

voltage for H_2-Air is 0.532 μJ and the corresponding average load resistor power is 5.32 μW. C_2H_4-N_2O has the highest energy per pulse corresponding to the higher area under the instantaneous power curve found in Fig. 19, followed by C_2H_4-Air and H_2-Air having the least energy per pulse for all fuel-oxidizer mixtures tested.

Phase 1 Power Density Analysis.

Table 7 contains values for the power density as calculated from the data by means of taking the peak load power from Fig. 19 also found in Table 7 and dividing it by the area of the plates (6.45×10^{-4} m^2) and the distance between the plates (0.0254 m).

Table 7. Phase 1: power density analysis from data

Fuel-Oxidizer Mixture	Peak Load Power (W)	Peak Power Density (W/m^3)
H_2-Air	4.26×10^{-5}	2.60
C_2H_4-Air	8.11×10^{-5}	7.07
C_2H_4-N_2O	7.68×10^{-5}	7.81

For all fuel-oxidizer mixtures, the values for peak power density are on the order of 1 W/m^3, significantly lower than the value of 10 MW/m^3 required for a feasible device[2].

Phase 1 Efficiency Analysis.

Considering the maximum value of energy extracted for each of the fuel-oxidizer mixtures from Fig. 20 at the maximum applied voltage for each fuel-oxidizer mixture (11.5 V for H_2-Air and C_2H_4-Air and 10.5 V for C_2H_4-N_2O), a resulting efficiency of the fuel-oxidizer mixtures relative to the respective detonation energy of each fuel-oxidizer mixture is found and shown in Table 8. For example, the maximum energy value obtained for C_2H_4-Air is 2.56 μJ per pulse at an applied voltage of

11.5 V. The resulting efficiency is $1.68 \times 10^{-8}\%$ relative to the 15.3 kJ per pulse from Table 4 for C_2H_4-Air. Clearly, an unseeded flow with a low applied electric field cannot produce a practical power level.

Table 8. Phase 1: efficiency analysis

Fuel-Oxidizer Mixture	Maximum Energy (μJ)	Efficiency
H_2-Air	1.31	$1.19 \times 10^{-8}\%$
C_2H_4-Air	2.56	$1.68 \times 10^{-8}\%$
C_2H_4-N_2O	4.59	$2.01 \times 10^{-8}\%$

4.2 Phase 2 Results for Applied Magnetic Field Only

The voltage, V_L (see Fig. 7), across a varying resistance was measured for the three different fuel-oxidizer mixtures. Resistances ranged from 100 Ω to 100 kΩ. Multiple pulses of data were taken for each resistance and each fuel-oxidizer mixture, but only the second pulse was used for calculation and presentation for similar reasons as discussed in phase one. Figure 21 shows example pulses for selected resistances for H_2-Air.

It can be seen that the voltage signal has a noticeably sharper and thinner early peak region (0-about 700 μs), in stark contrast with the broader region seen in phase one experiments (c.f., Fig. 13), but settled down to comparable values to those of phase one in a series of secondary and tertiary wave formations.

Phase 2: Gas Conductivity.

The gas conductivity for phase two was computed using Eq. 6. Figure 22 shows the conductivity of the fluid with respect to time for three selected load resistors (200 Ω, 2 kΩ, and 20 kΩ) for the three different fuel-oxidizer mixtures. Note that conductivity

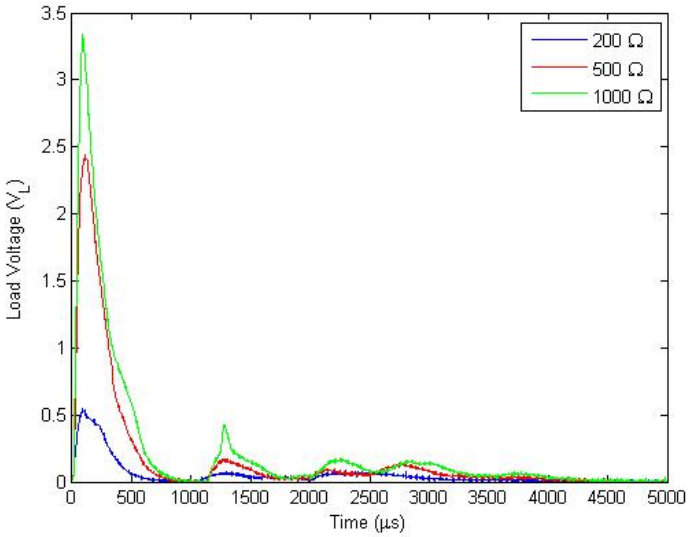

Figure 21. Phase 2: load voltage for multiple load resistances, H_2-Air

falls with time, as in phase one, but also with increased load resistance. The secondary wave formation seen in Fig. 22 was also commented on other researchers[1] (who offered no reason for the behavior).

The conductivity profiles seen in Fig. 22 are similar in shape to the voltage profile seen in Fig. 21. A comparison of phase one results with phase two shows that the conductivity profiles for the 3.0 V case (Fig. 15) closely approximates the 20 kΩ conductivities shown in Fig. 22. The conductivities should match closely because while there may be changes to flow properties in time, there should be little to no changes in flow properties between pulses or between test runs.

Figure 23 shows the instantaneous conductivity for all three fuel-oxidizer mixtures for the 1000 Ω load resistance. Figure 23 shows that peak conductivity are similar for all the fuel-oxidizer mixtures, approximately 0.0225 S/m. However, C_2H_4-N_2O has a significantly greater sustained conductivity than the other two fuel-oxidizer mixtures which are otherwise relatively close to each other over the entire duration of the pulse. The similar detonation temperatures as seen in Table 4 of the H_2-Air and C_2H_4-Air explains how the conductivities seen in Fig. 23 are similar for these two cases while

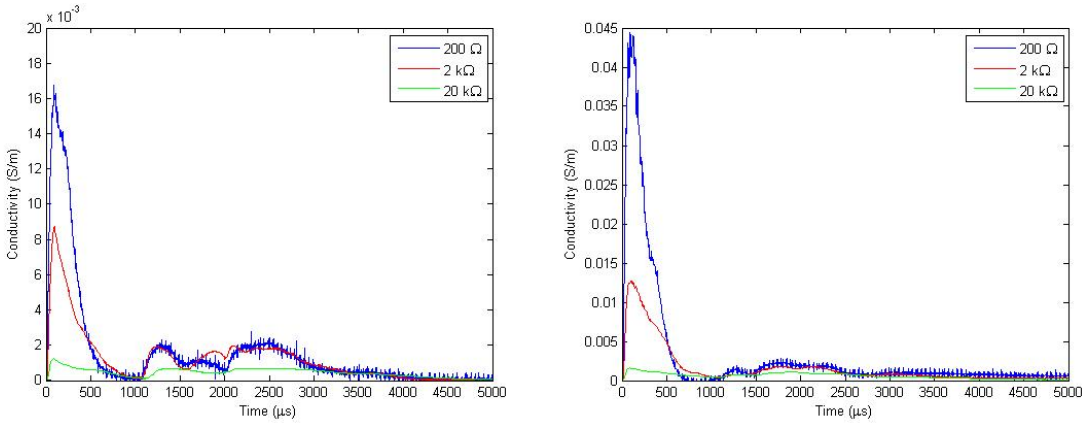

(a) H_2-Air

(b) C_2H_4-Air

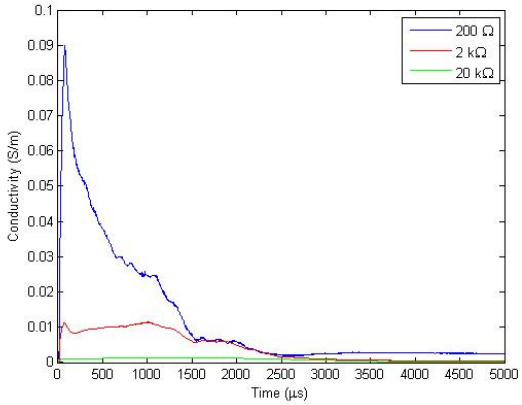

(c) C_2H_4-N_2O

Figure 22. Phase 2: instantaneous conductivity for selected load resistances, mixture specified

C_2H_4-N_2O was slightly higher. These values correspond roughly to the nearly zero value seen in other research[6] for a non-seeded case.

Instantaneous Power through Load Resistor, R_L.

Figure 24 shows instantaneous load power for the 200 Ω, 2 kΩ, and 20 kΩ, load resistors using Eq. 7. Figure 24a shows that power rises then falls with load resistances, indicating the existence of an optimum load resistance for maximum power extraction. Since the optimum load resistance is the load resistance equal to

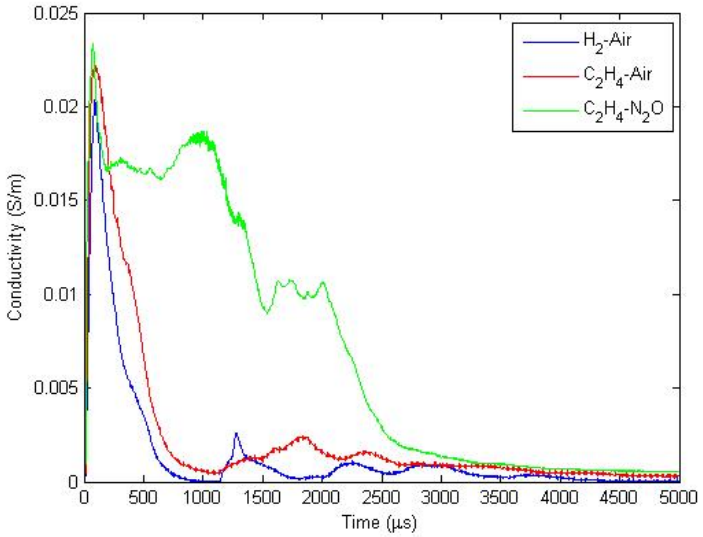

Figure 23. Phase 2: instantaneous conductivity for 1000 Ω load resistance, all mixtures

the internal resistance of the fluid, and the internal resistance of the fluid depends on the conductivity, one unique optimum resistance value for power extraction will be a compromise value. For the ethylene-oxidizer test cases (Figs. 24b and 24c), the power fell with increasing load resistance indicating the optimum load resistance for maximum power extraction to be less than or equal to 200 Ω for those two cases.

Figure 25 shows the instantaneous power for the 1000 Ω load resistance for all fuel-oxidizer mixtures. For H_2-Air and C_2H_4-Air, the instantaneous power profiles are similar while C_2H_4-N_2O profile is wide and sustained. Peak instantaneous power values for H_2-Air and C_2H_4-Air is about 0.013 W while the peak instantaneous power value for C_2H_4-N_2O is about 0.015 W, just slightly higher.

Energy Extracted through Load Resistor, R_L.

Figure 26 shows the load resistor energy per detonation pulse using Eq. 8 for the three fuel-oxidizer mixtures tested. In Fig. 26, notice that the energy rises and falls with load resistance, again indicating the existence of an optimum load resistance as seen in the instantaneous power figures. A variation with load resistance

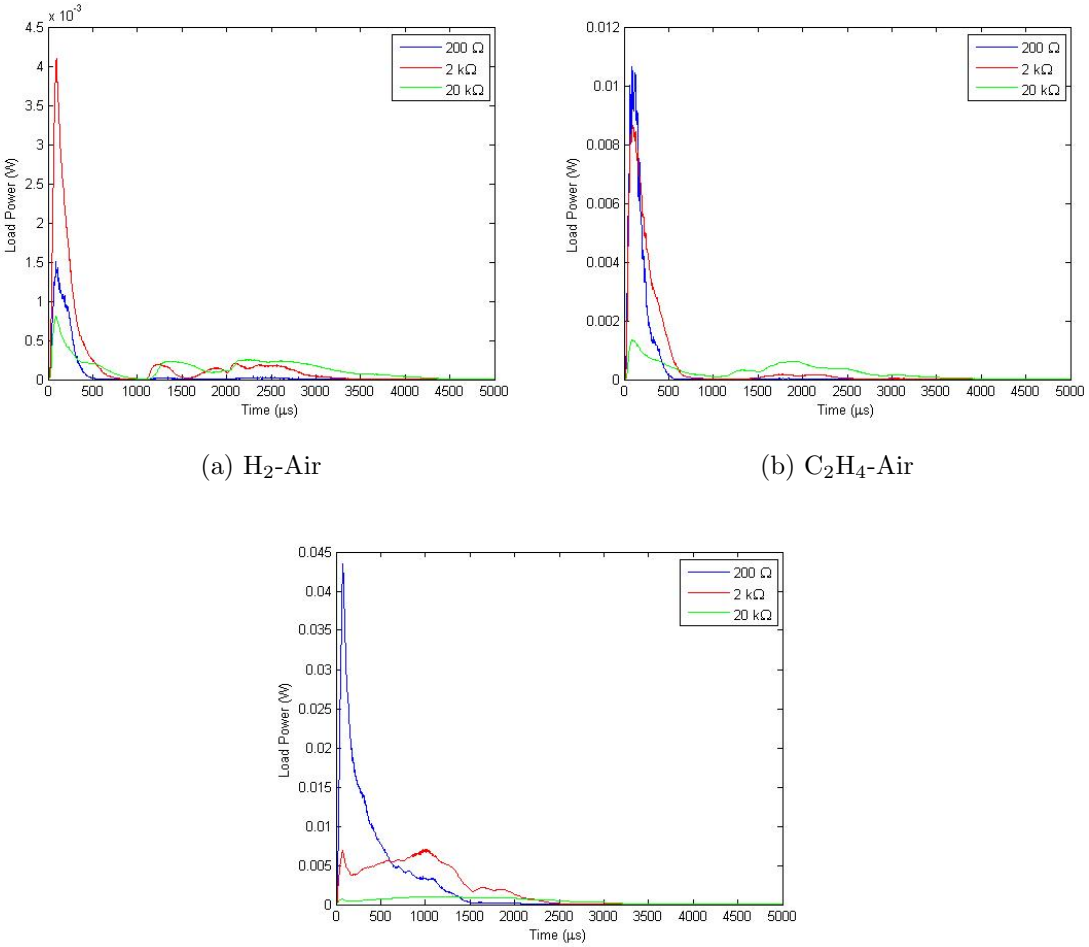

(a) H_2-Air

(b) C_2H_4-Air

(c) C_2H_4-N_2O

Figure 24. Phase 2: instantaneous power for selected load resistances, mixture specified

similar to that in Fig. 26 was seen in other works[1, 6] with similar conclusions made though values were significantly higher due to a strong applied electric field/calculated effective magnetic field.

From Fig. 26, C_2H_4-N_2O generates more energy per pulse compared to H_2-Air and C_2H_4-Air. This is likely due to the increased detonation temperature of C_2H_4-N_2O ($\sim$3800 K) compared to the detonation temperature of H_2-Air and C_2H_4-Air ($\sim$2800 K) as found in Table 4. Increased detonation temperatures increase the conductivity of the fluid as seen in Tables 1 and 2, and accordingly, the energy extracted from the

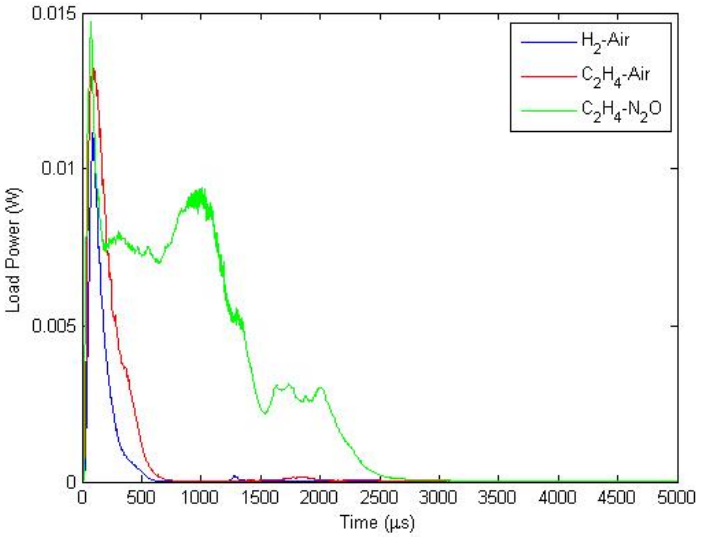

Figure 25. Phase 2: instantaneous power for 1000 Ω load resistance, all mixtures

flow.

The average power is solved for using Eq. 9 and is simply the energy values in Fig. 26 multiplied by 10 (= f). For example, in Fig. 26, the load resistor energy calculated for C_2H_4-Air for the 2 kΩ load resistance is 2.437 μJ, and the corresponding average load resistor power is 24.37 μW. The maximum energy value for load resistances tested for C_2H_4-Air was 3.246 μJ corresponding to a load resistance of 1000 Ω.

Effect of ϕ.

Fuel-oxidizer equivalence ratio, ϕ, testing was accomplished on the C_2H_4-N_2O test setup. Figure 27 shows the effect of ϕ on the energy extracted from the flow for three selected load resistances.

Multiple points were tested from a lean to rich mixture. A lean mixture is a mixture where the fuel-oxidizer mixture is less than the mass fraction of fuel for stoichiometric combustion. A rich mixture is a mixture where the fuel-oxidizer mixture is greater than the mass fraction of fuel for stoichiometric combustion. The first and last points encompass the bounds of the detonation, defined as the

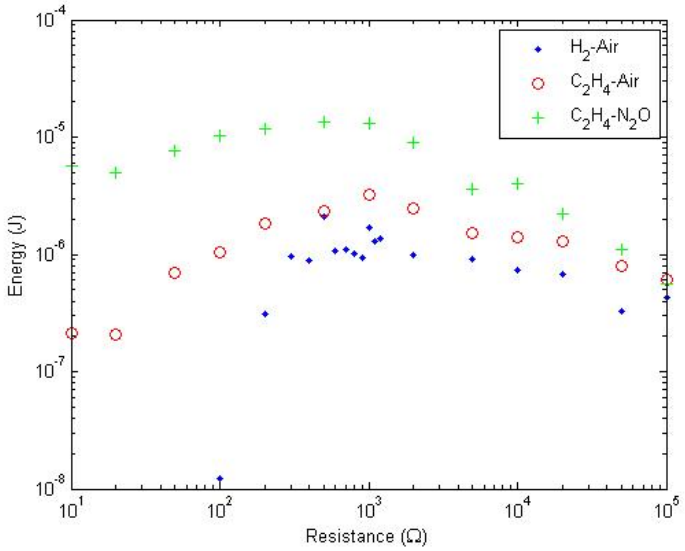

Figure 26. Phase 2: load resistor energy per pulse as a function of load resistance, all mixtures

fuel-oxidizer mixtures where the fuel-oxidizer mixture was barely detonable. The actual values of ϕ were unknown due to the inability on this setup to measure that parameter. While each individual set of points cannot be determined whether it is lean or rich, due to the test procedure outlined in Chapter 3, each set of points can be determined whether it is a more lean or more rich mixture compared to another set of points. This fact allows them to be plotted in an ordinal fashion as is shown in Fig 27.

Figure 27 shows that the energy extracted per pulse increases then decreases with ϕ, indicating the existence of an optimum ϕ for maximum energy extraction. This optimum value for ϕ occurs at the same value for all three resistances tested suggesting that it is independent of load resistance. Additionally, a lean fuel mixture favors the 1000 Ω resistance, compared to a rich fuel mixture which favors the 100 Ω resistance for maximum energy extraction. A possible reason for this is that richer fuel mixtures have a lower internal resistance of the fluid and in order to maximize energy extraction, the load resistance must be matched to the internal resistance of

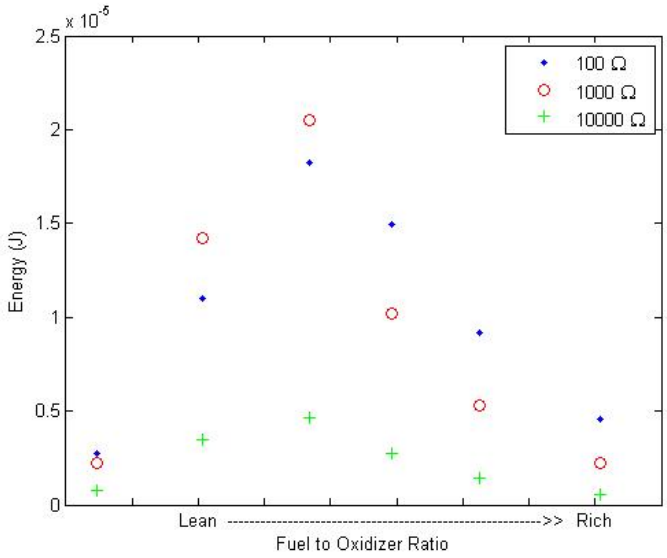

Figure 27. Effect of ϕ on energy extracted for C_2H_4-N_2O, selected load resistances, no seeding

the fluid.

Phase 2 Power Density Analysis.

Table 9 contains values for the power density as calculated by means of taking the peak load power from Fig. 25 shown in Table 9 and dividing it by the area of the plates (0.001824 m^2) and the average distance between the plates (0.02183 m) as measured for the split magnet device.

Table 9. Phase 2: power density analysis from data

Fuel-Oxidizer Mixture	Peak Load Power (W)	Power Density (W/m^3)
H_2-Air	0.0111	278.8
C_2H_4-Air	0.0132	331.5
C_2H_4-N_2O	0.0147	369.2

Assuming a nearly sonic flow velocity (M∼1) and using the values of speed of sound calculated by CEA[4] shown in Table 5, the flow velocity is then the value for

speed of sound. Using the peak value of conductivity for the 1000 Ω load resistance from Fig. 23 and shown in Table 10, a magnetic field of 0.2813 T, the assumed flow velocity for each fuel-oxidizer mixture, the power density using Eq. 15 are summarized in Table 10.

Table 10. Phase 2: power density analysis

Fuel-Oxidizer Mixture	Peak Conductivity (S/m)	Power Density (W/m^3) (Eq. 15)
H_2-Air	20.36×10^{-3}	479.5
C_2H_4-Air	22.18×10^{-3}	443.3
C_2H_4-N_2O	23.38×10^{-3}	662.0

For all fuel-oxidizer mixtures, the peak power density calculated from Eq. 15 is greater than the peak power density calculated from the peak power shown in Fig. 25. This difference in peak power density is likely due to three different effects. First, the nearly sonic flow assumption made to calculate the power density from Eq. 15 could cause the power density to be higher than it actually is. Second, there could be some uncertainty from the non-uniform field inside the channel (Fig. 9). Finally, the values for plate area and distance between the plates could be too high artificially creating a high mean effective volume. This uncertainty can be attributed to edge effects within the channel. Given the experimental (Table 9) and theoretical (Table 10) values for power density for C_2H_4-N_2O, if both the product of the area of the plates and distance between the plates and the value for flow velocity were reduced by 17.7% the values of power density would be equal. This reduction value is 16.5% and 9.3% for H_2-Air and C_2H_4-Air, respectively. All peak power density values calculated from Eq. 15 were on the order of 100 W/m^3 significantly lower than the value of 10 MW/m^3 required for feasible use[2].

Phase 2 Efficiency Analysis.

From the maximum value of energy extracted for each of the fuel-oxidizer mixtures taken from Fig. 26 at the optimal load resistance, a resulting efficiency of the fuel-oxidizer mixtures is found in Table 11 relative to the respective detonation energies found in Table 4 of each fuel-oxidizer mixture. For example, the maximum energy value obtained for C_2H_4-Air is 3.25 μJ per pulse at a load resistance of 1000 Ω. The resulting efficiency is 2.12×10^{-8}% relative to the 10.4 kJ per pulse found in Table 4 for C_2H_4-Air. Again as seen in phase one, an unseeded flow with a low applied electric field cannot produce a practical power level.

Table 11. Phase 2: efficiency analysis

Fuel-Oxidizer Mixture	Maximum Energy (μJ)	Efficiency
H_2-Air	2.10	1.90×10^{-8}%
C_2H_4-Air	3.25	2.12×10^{-8}%
C_2H_4-N_2O	13.5	5.94×10^{-8}%

4.3 Phase 3 Results for Applied Magnetic Field with Flow Seeding

The voltage, V_L, across a varying resistance was measured for the ethylene fuel-oxidizer mixtures with seed added to the flow. H_2-Air was omitted from this phase of testing in order to focus on ethylene testing which showed higher energy extraction results seen in Fig. 26. Figure 28 shows example seeding pulses for two different seeding materials (water and aqueous NaCl) for C_2H_4-N_2O.

Resistance values were tested ranging from 100 Ω to 100 kΩ. Pulses of data were taken for each resistance and each fuel-oxidizer mixture, but only the second pulse was used for calculation and presentation due to the same trends seen in phases one and two. It can be seen in Fig. 28 that the phase three voltage signal is similar to

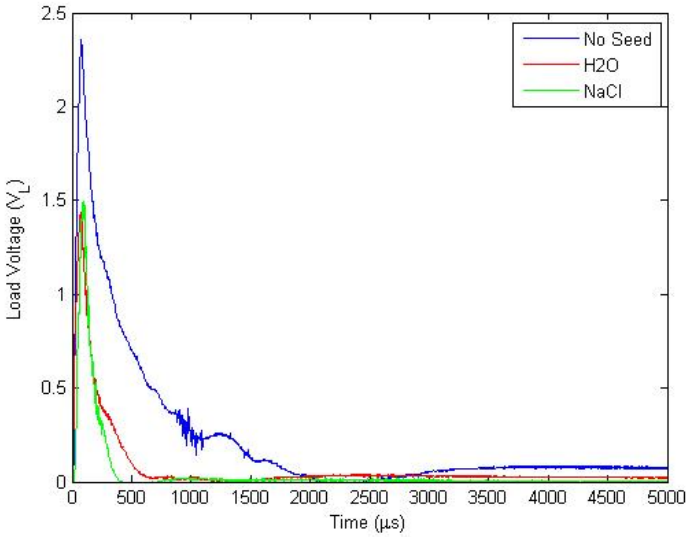

Figure 28. Phase 3: load voltage for initial seed testing with NaCl, R_L = 1000 Ω

the shape seen in phase two (Fig. 21) though not matching magnitude. Following are details of the seeded flow experiment.

Initial Seed Testing with NaCl.

Initial seed testing with NaCl was accomplished on the C_2H_4-N_2O setup. Two different seeding materials (water and aqueous NaCl) were examined in this testing. For each seed, approximately 2 mL were added to the tube, allowed to coat the inside and the excess removed from the tube. Figure 29 shows the energy extracted for the initial seed testing using NaCl calculated using Eq. 8. Three resistance values were tested for each case: 100 Ω, 1000 Ω, and 10 kΩ.

For all three resistances tested and all cases tested, the energy extracted (using Eq. 8), by the split magnet device with seeding was less than the no seeding case (Fig. 29) and the NaCl caused a lower energy than water alone. The author ascribes the lower values obtained from the NaCl seeding cases to three effects. First, the water and aqueous NaCl were added at the temperature of the test facility which was approximately 22°C. Detonation occurred shortly after the seed was added not

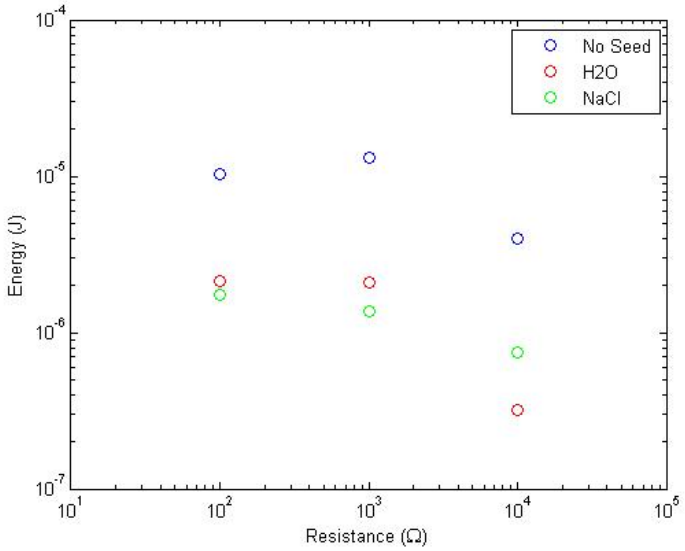

Figure 29. Phase 3: load resistor energy for initial seed testing with water and aqueous NaCl, C_2H_4-N_2O, selected load resistances

allowing time for the water to evaporate. Since the temperature of the detonation was at approximately 3800 K, the addition of either seed into the flow has the effect of cooling the flow upon contact. Assuming 1 mL of seeding material remained in the tube, that results in 1 g or 0.0556 mol of water added to the tube. When the amount of moles per detonation is only 0.179 mol, by the ideal gas law, the seed adds approximately 31% more molecules to the flow which, for equilibrium temperature, will require energy to heat them. Assuming that the molecules in the flow and the seed molecules have the same specific heat capacity, that would result in a 24% loss in energy for ionization. Second, the water and aqueous NaCl were added prior to detonation. This means that the molecules needed to be accelerated by the flow via momentum transfer which has a similar effect of removing energy from the flow. Also noted is that the NaCl in aqueous solution did have an effect on the flow since the values obtained by using the aqueous NaCl were lower than the values obtained by water alone as a seed. Finally, it is noted that a chlorine ion has the highest electron afffinity on the periodic table at 3.61 eV[25]. Compared to other ions which

are present, sodium (0.548 eV[26]) and oxygen (1.46 eV[27]) chlorine is more likely to attach to an electron and create a negative ion removing an electron from the available electrons in the flow. Due to these three reasons, the decision was made to switch to a different seeding material. K_2CO_3 was selected as the next and final seeding material.

Seeding with Potassium Carbonate.

C_2H_4-Air.

Phase three testing for C_2H_4-Air with K_2CO_3 as a seed was done to determine its effectiveness. Two different locations for dry seed material introduction were tested, 1.07 meters and 1.22 meters (see Fig. 30). Approximately 0.25 g of seed material was added to the tube for each test point. Figure 30 shows the load resistor energy for a single pulse for the two dry seed introduction locations tested compared with the results found in phase two with no seed added for selected load resistances.

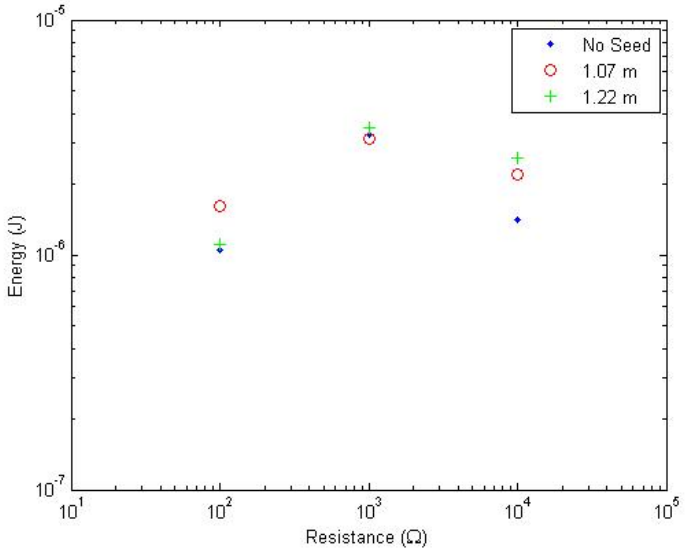

Figure 30. Phase 3: load resistor energy for C_2H_4-Air seed material testing with K_2CO_3 for selected load resistances

In most cases, introduction of the dry K_2CO_3 (Fig. 30) increased the energy

extracted by the split magnet device. This same effect would be expected using any number of fuel-oxidizer mixtures on the same setup. Based on the data in Fig. 30, introduction of the seeding material later in the tube favored higher load resistances while earlier introduction of the seeding material favored lower load resistances.

C_2H_4-N_2O.

Phase three testing for C_2H_4-N_2O with K_2CO_3 as a seed material was done to determine the best conditions for flow seeding. For dry seeded cases, approximately 0.5 g of seeding material was added and for wet seeded cases, the same process used for testing with NaCl was used. Multiple data points were taken to determine whether

- a dry powder or aqueous solution should be used,
- location of the introduction of the seed matters, and
- changing ϕ has any effect on the energy collected by the split magnet device.

The voltage, V_L, across a resistance of 10 kΩ was measured instead of the 1000 Ω load resistor. While a load resistance of 1000 Ω is closer to the load resistance for maximum energy extraction (Fig. 26), there is no concern testing the 10 kΩ because such testing will show the same trends for the 1000 Ω resistance and differ only slightly from the 1000 Ω energy extracted value. Data points were collected with a lean mixture, defined as a fuel-oxidizer mixture where the mass fraction of fuel is less than the stoichiometric mass fraction of fuel, unless otherwise specified.

The first set of data (Fig. 31) shows the effect on energy extraction of dry powder or aqueous solution application. Measurements, shown along the x-axis are measured from the fuel-oxidizer injectors (also coincident with the entrance of the tube), (Fig. 12).

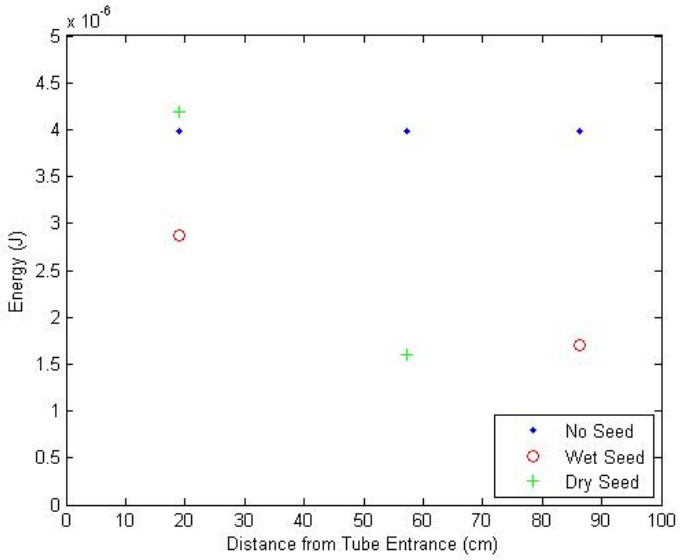

Figure 31. Phase 3: seed testing with K_2CO_3, R_L = 10 kΩ

Figure 31 shows that for both cases, dry powder and saturated aqueous solution seeding, the later the seed was introduced the lesser the energy extracted. As seen with the NaCl testing (Fig. 29), the aqueous solution seed did worse than the dry powder seed at the same location. Both the dry powder and aqueous solution seeds introduced at 57.2 cm and 86.4 cm, respectively resulted in less energy extracted when compared to a non-seeded case.

Regarding wet versus dry seeding, applying the K_2CO_3 salt to the interior of the tube as a saturated aqueous solution and allowing the water to evaporate did not increase the energy extracted by an unseeded split magnet device. A likely reason for the decrease in energy extraction seen is that evaporated water molecules existed in the PDT. The excess water vapor would have a deleterious effect on the flow energy similar to that of the water molecules in liquid phase. Previous testing (Fig. 29) showed similar results when water was added into the PDT. Since water molecules have a higher heat capacity (∼2x) than other molecules in the flow, it takes more energy to increase their molecular temperature. Excess water molecules in the flow require more energy to be taken from the flow, energy which could otherwise be used

to increase the ionization of the particles within the flow. Additional water molecules in the PDT can also have a cooling effect which leads to a lower conductivity and lower energy extracted.

Effect of ϕ.

The effect of ϕ on energy extracted was also tested with seeding. Figure 32 shows the voltage traces for a lean or rich mixture with dry seeding.

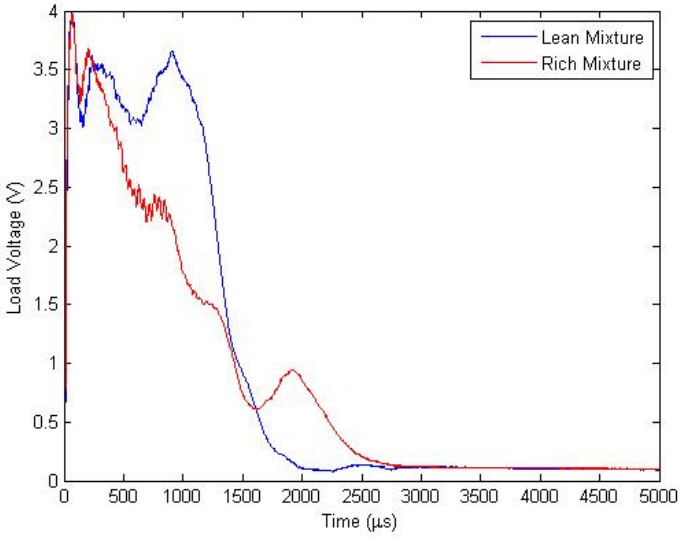

Figure 32. Phase 3: dry seed testing with K_2CO_3, lean and rich mixtures, $R_L = 10$ kΩ

Both cases, tested with dry K_2CO_3 seed application at 57.2 cm, showed lower energy extracted than the no seeding case, but this effect could be due to the location where the seed was applied. More importantly only 1.60 μJ were extracted out of the lean mixture case compared to 1.23 μJ in the rich mixture case calculated from Eqs. 7 and 8. A possible reason for the lower value for the rich mixture case is that for the rich mixture, the selected rich test mixture was farther away from the optimal ϕ where the maximum energy extraction occurs, eg., further to the right in Fig. 27, resulting in a lower energy extracted.

Phase 3 Efficiency.

Considering the maximum value of energy extracted for each of the fuel-oxidizer mixtures tested in Phase 3 summarized in Table 12 from Figs. 30 and 31 at the optimal load resistance of those tested for each fuel-oxidizer mixture, a resulting efficiency of the fuel-oxidizer mixtures is found in Table 12 relative to the respective detonation energy of each fuel-oxidizer mixture. For example, the maximum energy value obtained for C_2H_4-Air is 3.48 μJ per pulse at a load resistance of 1000 Ω. The resulting efficiency is $2.28 \times 10^{-8}\%$ relative to the 10.4 kJ per pulse found in Table 4 for C_2H_4-Air.

Table 12. Phase 3: efficiency analysis

Fuel-Oxidizer Mixture	Maximum Energy (μJ)	Efficiency
C_2H_4-Air	3.48	$2.28 \times 10^{-8}\%$
C_2H_4-N_2O	4.19	$1.83 \times 10^{-8}\%$

Since the C_2H_4-N_2O seed testing was done at a load resistance of 10 kΩ, it will need to be compared to the value obtained for the 10 kΩ load resistance case in phase two seen in Fig. 26 (3.98 μJ). When compared to the value found in Table 12, the value obtained in phase two was less than the value in Table 12 indicating a increase in power extraction due to K_2CO_3 seeding for C_2H_4-N_2O. Note that the C_2H_4-N_2O testing was done with a load resistor of 10 kΩ which was not the load resistance with the highest energy extracted and cannot be compared with the phase two efficiency calculations found in Table 11.

V. Conclusions and Recommendations

5.1 Electric and Magnetic Field Performance

For a relatively weak electric field (0.20 to 4.53 V/cm) or magnetic field (0.2813 T) applied across collector plates situated in an unseeded PDT experiencing a detonation event, load resistor energy efficiency is on the order of 10^{-8}%, far too low for feasible use. However, since the minimum ignition energy required for H_2-Air ignition is on the order of 1 μJ[5], the energy extracted by the split magnet device may be enough to feed back to the ignition system for the PDT to self-sustain the detonation process. Research done in this thesis shows that 1000 Ω seems to be the optimum resistance for the fuel-oxidizer mixtures tested which suggests impedance matching of the load resistance to the internal resistance of the fluid increases the energy extracted from an MHD device. A seeded PDT with the same relatively weak electric field and magnetic field with sodium chloride or potassium carbonate also yielded load resistor energy efficiency is on the order of 10^{-8}%, still far too low for feasible use. The efficiencies seen in phase three are on the same order of magnitude as phases one and two, leading to the belief that the methodology itself of seeding done in this thesis coupled with the relatively weak magnetic field of the split magnet device did not show large increases in energy extraction due to seeding. The greatest benefit from seeding was seen in C_2H_4-Air with a percent increase of approximately 7% in energy extracted. C_2H_4-N_2O trailed slightly with an approximate 5% increase in energy extracted. Testing of different values for fuel-oxidizer equivalence ratio, ϕ, showed that an optimal ϕ exists and is independent of load resistance.

5.2 Feasibility

In order to meet the 10 MW/m^3, the required power density for acceptable size[2], either conductivity, gas velocity, magnetic field strength, or any combination of the three variables must be increased. The current limit on magnetic field strength of a permanent magnet is approximately 1 T at the surface of the magnet. The gas velocity is limited by the speed of sound which in this case was approximately 1 km/s. The corresponding required conductivity using those two limits is 40 S/m which is attainable with a 0.001 cesium mole fraction[1, 6]. While results from the testing accomplished in this thesis did not show favorable energy extraction values for feasible use, the fact that the 40 S/m is attainable[1, 6] shows promise for continued research.

5.3 Recommendations for Future Research

The following sections have recommendations for areas of future research related to this thesis.

Field Strength.

An obvious method to increase the energy extracted from the flow based on the conclusions above would be to increase the field strength of both the electric field or the magnetic field. Since the electric field does not provide any usable work from the flow (all the power comes from the attached voltage source and only provides theoretical energy extracted results for an induced electric field of equal magnitude), continuing with the electric field experiments does not yield any meaningful results for MHD applications.

Conductivity.

Other methods to increase the energy extracted from the flow may prove to be more feasible. Two other parameters can be modified in order to increase the energy extracted, the velocity of the flow, v, and the conductivity of the flow, σ. In order to increase the conductivity and the power extracted using different flow seeding materials, elements with lower ionization energies such as cesium or francium would be needed. These seeding materials will ionize with less energy and increase the electron density of the flow. This increase in electron density would increase the efficiency of the system, by means of increasing conductivity, as would an increase in the magnitude of the magnetic field. However, these seeding materials are not as readily available or as safe to handle as the seeding materials used in this thesis.

Flow Velocity.

Higher values of energy can be extracted by increasing the flow velocity. Increases in flow velocity have a direct affect on the magnitude of the induced electric field. Increases in the electric field (induced or applied) increase the energy which can be extracted as seen in phase one experiments. Experiments that would increase the electron velocity and increase the induced electric field should increase the energy extracted.

Fuel-Oxidizer Equivalence Ratio.

Higher values of energy could be extracted by matching ϕ to the optimal ϕ. More testing with various different values for ϕ needs to be done in order to determine the best ϕ for the greatest energy extraction.

Impedance Matching.

Finally, impedance matching the load resistances with the theoretical value of the internal resistance of the fluid should also lead to higher power output.

Future Work.

Future work will entail research to maximize energy extraction by varying flow parameters such as fuel to oxidizer ratio, fuel-oxidizer mixtures, and flow seeding materials such as cesium-hydroxide or potassium stearate using different methods such as direct injection or different solutions than those tested in this thesis.

Bibliography

1. R. J. Litchford, B. R. Thompson, and J. T. Lineberry, "Pulse detonation magnetohydrodynamic power," *Journal of Propulsion and Power*, vol. 16, no. 2, pp. 251–262, 2000.

2. M. Mitchner and C. H. Kruger, *Partially Ionized Gases*, vol. 8. New York: John Wiley and Sons, Inc, 1973.

3. J. M. Yos, "Transport properties of nitrogen, hydrogen, oxygen, and air to 30,000°k," RAD-TM-63-7, March 1963.

4. S. Gordon and B. J. McBride, "Chemical equilibrium with applications[computer software]," Cleveland, OH, 1994.

5. A. Kumamoto, H. Iseki, R. Ono, and T. Oda, "Measurement of minimum ignition energy in hydrogen-oxygen-nitrogen premixed gas by spark discharge," *Journal of Physics: Conference Series*, vol. 301, 2011.

6. R. J. Litchford, "Integrated pulse detonation propulsion and magnetohydrodynamic power," NASA/TP-2001-210801, January 2001.

7. M. Matsumoto, M. Tomoyuki, and O. Yoshihiro, "Numerical studies of flow behavior and performance in a pulse-detonation-driven mhd generator," AIAA-2007-4130, 38th AIAA Plasmadynamics and Lasers Conf., 25-28 June 2007. Miami, Florida.

8. R. J. Litchford, B. R. Thompson, and J. T. Lineberry, "Pulse detonation mhd experiments," AIAA-98-2918, 29th AIAA Plasmadynamics and Lasers Conf., 15-18 June 1998. Albuquerque, NM.

9. J.-L. Cambier, "Mhd power extraction from a pulse detonation engine," AIAA-98-3876, 34th AIAA J. Prop. Conf., 13-15 July 1998. Cleveland, OH.

10. K. I. Teope, P. I. King, F. R. Schauer, and J. L. Hoke, "Experimental magnetohydrodynamic energy extraction from a pulsed detonation tube," AIAA-2015-1348, 53rd AIAA Aerospace Sciences Meeting, 5-9 January 2015. Kissimmee, FL.

11. S. F. R., C. L. Miser, K. C. Tucker, B. R. P., and J. L. Hoke, "Detonation initiation of hydrocarbon-air mixtures in a pulsed detonation engine," AIAA-2005-1343, 43rd AIAA Aerospace Sciences Meeting, 10-13 January 2005. Reno, NV.

12. C. Li, K. Kailasanath, and G. Patnaik, "A numerical study of flow field evolution in a pulsed detonation engine," AIAA-2000-0314, 38th AIAA Aerospace Sciences Meeting, 10-13 January 2000. Reno, NV.

13. S. Eidelman and G. W., "Pulsed detonation engine experimental and theoretical review," AIAA-92-3168, 28th AIAA J. Prop. Conf., 06-08 July 1992. Nashville, TN.

14. S. Eidelman, "Pulse detonation engine: A status review and technology development roadmap," AIAA-1997-2740, 33rd AIAA J. Prop. Conf., 06-09 July 1997. Seattle, WA.

15. F. Schauer, J. Stutrud, and R. Bradley, "Detonation initiation studies and performance results for pulsed detonation engine applications," AIAA-2001-1129, 39th AIAA Aerospace Sciences Meeting, 8-11 January 2001. Reno, NV.

16. J.-L. Cambier and J. K. Tegnér, "Strategies for pulsed detonation engine

performance optimization," *Journal of Propulsion and Power*, vol. 14, no. 4, pp. 489–498, 1998.

17. S. Eidelman and X. Yang, "Analysis of the pulse detonation engine efficiency," AIAA-1998-3877, 34th AIAA J. Prop. Conf., 13-15 July 1998. Cleveland, OH.

18. R. J. Litchford, "Development of a gas-fed pulse detonation research engine," AIAA-2001-3814, 37th AIAA J. Prop. Conf., 8-11 July 2001. Salt Lake City, UT.

19. C. F. Zeineh, C. L. K., T. Roth, A. R. Karagozian, and J.-L. Cambier, "Magnetohydrodynamic augmentation of pulsed detonation rocket engines," *Journal of Propulsion and Power*, vol. 28, no. 1, pp. 146–159, 2012.

20. N. Harada, J. Ikewada, and Y. Terasaki, "Basic studies on an mhd accelerator," AIAA-2002-2175, 33rd AIAA Plasmadynamics and Lasers Conf., 21-23 May 2002. Maui, HI.

21. M. Anwari, S. Takahashi, and N. Harada, "Performance study of a magnetohydrodynamic accelerator using air-plasma as working gas," *Energy conversion and management*, vol. 46, no. 15, pp. 2605–2613, 2005.

22. J.-L. Cambier and D. Lofftus, "Mhd power generation from a pulse detonation rocket engine," AIAA-2002-2115, 14th International Conference on MHD Power Generation, 20-23 May 2002. Maui, Hawaii.

23. B. J., *Metal Ions in Solution*. New York, NY: Ellis Horwood, 1978.

24. W. C. de Baat, "Sur l'acide dithionique et ses sels," *Recl. Travl. Chim. Pays-Bas*, vol. 45, pp. 237–244, 1926.

25. U. Berzinsh, M. Gustafsson, D. Hanstorp, A. Klinkmüller, U. Ljungblad, and

A.-M. Mårtensson-Pendrill, "Isotope shift in the electron affinity of chlorine," *Phys. Rev. A*, vol. 51, pp. 231–238, Jan 1995.

26. H. Hotop and W. Lineberger, "Binding energies in atomic negative ions ii," *J. of Phys. and Chem. Ref. Data*, vol. 14, p. 731, 1985.

27. W. Chaibi, R. Peláez, C. Blondel, C. Drag, and C. Delsart, "Effect of a magnetic field in photodetachment microscopy," *The European Phys. J. D*, vol. 59, p. 29, 2010.

Vita

Captain Kaz Teope graduated from Schaumburg High School in Schaumburg, Illinois. He attended the United States Air Force Academy in Colorado Springs, Colorado where he graduated with a Bachelor of Science degree in Aeronautical Engineering in May 2009. He was commissioned at the Air Force Academy where he graduated on the Dean's List.

He was first assigned to Kirtland AFB to the Space Vehicles Directorate for the Air Force Research Laboratory where he specialized in inter and intrasatellite optical networking and trained future AFRL satellite operators for the ANGELS satellite and future satellite programs.

While at Kirtland, Captain Teope graduated from the University of New Mexico in May 2013 with a Master of Business Administration focusing in Operations Management and Marketing. He was accepted into the USAFA Faculty Pipeline program to pursue a Master of Science degree in Aeronautical Engineering at the Air Force Institute of Technology with a follow-on assignment to the USAF Academy to teach for the Department of Engineering Mechanics.

REPORT DOCUMENTATION PAGE

Form Approved
OMB No. 0704–0188

1. REPORT DATE *(DD–MM–YYYY)*	2. REPORT TYPE	3. DATES COVERED *(From — To)*
26–03–2015	Master's Thesis	Sep 2013 — Mar 2015

4. TITLE AND SUBTITLE

Experimental Magnetohydrodynamic Energy Extraction from a Pulsed Detonation

5a. CONTRACT NUMBER

5b. GRANT NUMBER

5c. PROGRAM ELEMENT NUMBER

6. AUTHOR(S)

Kaz I. Teope, Capt, USAF

5d. PROJECT NUMBER

5e. TASK NUMBER

5f. WORK UNIT NUMBER

7. PERFORMING ORGANIZATION NAME(S) AND ADDRESS(ES)

Air Force Institute of Technology
Graduate School of Engineering and Management (AFIT/EN)
2950 Hobson Way
WPAFB OH 45433-7765

8. PERFORMING ORGANIZATION REPORT NUMBER

AFIT-ENY-MS-15-M-224

9. SPONSORING / MONITORING AGENCY NAME(S) AND ADDRESS(ES)

Air Force Research Lab Aerospace Directorate
Combustion Branch, Turbine Engine Division
1790 Loop Road North
WPAFB OH 45433-7765

10. SPONSOR/MONITOR'S ACRONYM(S)

AFRL/RQTC

11. SPONSOR/MONITOR'S REPORT NUMBER(S)

12. DISTRIBUTION / AVAILABILITY STATEMENT

DISTRIBUTION STATEMENT A:
APPROVED FOR PUBLIC RELEASE; DISTRIBUTION UNLIMITED.

13. SUPPLEMENTARY NOTES

14. ABSTRACT

The high MWatt power available in a fuel-fed detonation wave, which contains combustion ions in the trailing gas, provides an opportunity for external power extraction via electromagnetically forced charged particle drift. Sets of experiments were accomplished using a pulsed detonation tube, extracting power across a load resistor in an electrical circuit with an applied electric or magnetic field to determine what magnitude of gas conductivity and power extraction could be attained from an unseeded or seeded pulsed detonation driven combustion. Due to the low magnetic field strength, even with flow seeding, the power extracted in this research was not enough for practical use. However, theoretical calculations with higher magnetic field strength and greater gas conductivity than was found in this research show promise for continued research. Future work would entail use of a stronger magnetic field to increase power extraction.

15. SUBJECT TERMS

Magnetohydrodynamic,Pulsed Detonation,Energy Extraction

16. SECURITY CLASSIFICATION OF:			17. LIMITATION OF ABSTRACT	18. NUMBER OF PAGES	19a. NAME OF RESPONSIBLE PERSON
a. REPORT	b. ABSTRACT	c. THIS PAGE			Dr. P. I. King, AFIT/ENY
U	U	U	UU	79	19b. TELEPHONE NUMBER *(include area code)* (937) 785-3636, x4628; paul.king@afit.edu